

2

NAVAL POSTGRADUATE SCHOOL Monterey, California

AD-A262 092



S DTIC
ELECTE
APR 01 1993
D
E

THESIS

MODIFICATION AND CALIBRATION OF
THE NAVAL POSTGRADUATE SCHOOL
ACADEMIC WIND TUNNEL

by

Robert L. Baldocchi

Thesis Advisor:

Louis V. Schmidt

Approved for public release; distribution is unlimited

98 8 31 134

93-06695

Unclassified

Security Classification of this page

REPORT DOCUMENTATION PAGE				
1a Report Security Classification: Unclassified		1b Restrictive Markings		
2a Security Classification Authority		3 Distribution/Availability of Report		
2b Declassification/Downgrading Schedule		Approved for public release; distribution is unlimited.		
4 Performing Organization Report Number(s)		5 Monitoring Organization Report Number(s)		
6a Name of Performing Organization Naval Postgraduate School	6b Office Symbol (if applicable) 31	7a Name of Monitoring Organization Naval Postgraduate School		
6c Address (city, state, and ZIP code) Monterey CA 93943-5000		7b Address (city, state, and ZIP code) Monterey CA 93943-5000		
8a Name of Funding/Sponsoring Organization	6b Office Symbol (if applicable)	9 Procurement Instrument Identification Number		
Address (city, state, and ZIP code)		10 Source of Funding Numbers		
		Program Element No	Project No	Task No
		Work Unit Accession No		
11 Title (include security classification) MODIFICATION AND CALIBRATION OF THE NAVAL POSTGRADUATE SCHOOL ACADEMIC WIND TUNNEL				
12 Personal Author(s) Robert L. Baldocchi				
13a Type of Report Master's Thesis	13b Time Covered From To	14 Date of Report (year, month, day) 1992, December, 17	15 Page Count 83	
16 Supplementary Notation The views expressed in this thesis are those of the author and do not reflect the official policy or position of the Department of Defense or the U.S. Government.				
17 Cosati Codes		18 Subject Terms (continue on reverse if necessary and identify by block number)		
Field	Group	Subgroup	Damping screen, pressure variation, flow angularity, turbulence intensity	
19 Abstract (continue on reverse if necessary and identify by block number)				
<p>Since the early 1980's, the Academic Wind Tunnel has operated with only one half its designed power section. Resultant flow qualities have limited the use of this facility. A damping screen was installed in the settling chamber to reduce the level of turbulence intensity in the tunnel. Following this modification, calibration measurements in the vertical centerplane were performed to document flow conditions in the test section. The tunnel calibration investigated lateral pressure variations, flow angularity, and turbulence intensity and included an airspeed calibration. When available results were compared to data from calibrations performed before the tunnel modification. Results indicate the total and static pressure lateral variation is within 1.0%, angular variation of approximately $\pm 1.0^\circ$ exists in the test section, and a 25.0% reduction in turbulence intensity was obtained due to the presence of the damping screen. Flow separation in the diffuser is believed to be influencing total pressure oscillation in the test section.</p>				
20 Distribution/Availability of Abstract <input checked="" type="checkbox"/> unclassified/unlimited <input type="checkbox"/> same as report <input type="checkbox"/> DTIC users		21 Abstract Security Classification Unclassified		
22a Name of Responsible Individual Louis V. Schmidt		22b Telephone (include Area Code) (408) 646-2491	22c Office Symbol Code 31/Sc	

Approved for public release; distribution is unlimited.

Modification and Calibration
of the Naval Postgraduate School
Academic Wind Tunnel

by

Robert L. Baldocchi
Lieutenant, United States Navy
B.S., United States Naval Academy, 1983

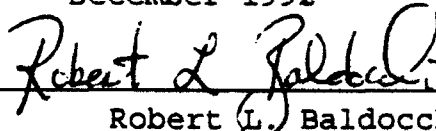
Submitted in partial fulfillment
of the requirements for the degree of

MASTER OF SCIENCE IN AERONAUTICAL ENGINEERING

from the

NAVAL POSTGRADUATE SCHOOL
December 1992

Author:




Robert L. Baldocchi

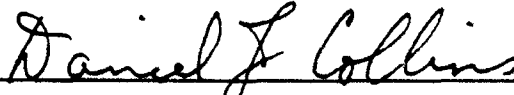
Approved by:



Louis V. Schmidt, Thesis Advisor



Richard M. Howard, Second Reader



Daniel J. Collins, Chairman
Department of Aeronautics and Astronautics

ABSTRACT

Since the early 1980's, the Academic Wind Tunnel has operated with only one half its designed power section. Resultant flow qualities have limited the use of this facility. A damping screen was installed in the settling chamber to reduce the level of turbulence intensity in the tunnel. Following this modification, calibration measurements in the vertical centerplane were performed to document flow conditions in the test section. The tunnel calibration investigated lateral pressure variations, flow angularity, and turbulence intensity and included an airspeed calibration. When available results were compared to data from calibrations performed before the tunnel modification. Results indicate the total and static pressure lateral variation is within 1.0%, angular variation of approximately $\pm 1.0^\circ$ exists in the test section, and a 25.0% reduction in turbulence intensity was obtained due to the presence of the damping screen. Flow separation in the diffuser is believed to be influencing total pressure oscillation in the test section.

Accession For	
NTIS CRA&I	<input checked="" type="checkbox"/>
DTIC TAB	<input type="checkbox"/>
Unannounced	<input type="checkbox"/>
Justification	
By	
Distribution /	
Availability Codes	
Dist	Avail and/or Special
A-1	

TABLE OF CONTENTS

I. INTRODUCTION	1
A. THE ISSUE	1
B. THE MODIFICATION	4
C. WIND TUNNEL CALIBRATION	6
II. EXPERIMENTAL PROCEDURES	9
A. LATERAL PRESSURE MEASUREMENTS	9
1. Data Acquisition	13
B. LONGITUDINAL PRESSURE MEASUREMENTS	15
C. FLOW ANGULARITY MEASUREMENTS.....	15
1. Data Acquisition	26
D. AIRSPEED CALIBRATION	33
1. Data Acquisition	35
E. TURBULENCE MEASUREMENTS	35
1. Data Acquisition	41
III. RESULTS	48
A. TUNNEL TEMPERATURE	48
B. TOTAL PRESSURE FLUCTUATIONS	49
C. MAXIMUM DYNAMIC PRESSURE	51
D. LATERAL PRESSURE VARIATION	52

E. FLOW ANGULARITY	54
F. AIRSPEED CALIBRATION	64
G. TURBULENCE INTENSITY	66
IV. CONCLUSIONS/RECOMMENDATIONS	71
A. LATERAL PRESSURE VARIATION	71
B. LONGITUDINAL PRESSURE VARIATION	71
C. FLOW ANGULARITY	72
D. TUNNEL TURBULENCE	73
E. CLOSING REMARKS	74
LIST OF REFERENCES	75
INITIAL DISTRIBUTION LIST	76

ACKNOWLEDGEMENT

I wish to thank the following Department of Aeronautics and Astronautics personnel whose contributions made this investigation possible.

Antonio Cricelli - Computer Engineer
Pat Hickey - Laboratory Supervisor
Don Harvey - Metal Model Maker
Ron Ramaker - Wood and Plastics Model Maker
John Moulton - Metal Model Maker
Jan Klienschmidt - Education Technician

I also wish to thank Professor Lou Schmidt, Associate Professor Rick Howard and Associate Professor Garth Hobson for their guidance and encouragement.

The final acknowledgement is reserved for Alan G. McGuire, the department's Aeronautical Engineer. Without his friendship, support and guidance this project would never have been completed.

I. INTRODUCTION

The most controversial laboratory facility within the Department of Aeronautics and Astronautics is the Naval Postgraduate School's 3.5' x 5.0' Academic Wind Tunnel. The faculty and staff are divided on the subject of the future use of the tunnel as an educational and experimental device. Without the benefit of a recent and thorough tunnel calibration following a major tunnel modification, opponents have lobbied for the removal of the wind tunnel facility. The purpose of this thesis is to perform and document a complete tunnel calibration and provide results as evidence for either side of this dispute.

A. THE ISSUE

The Academic Wind Tunnel is a low-speed, closed-circuit wind tunnel. Located in the southwest corner of Halligan Hall, it measures 75.0 feet in length, 15.0 feet in width and 60.0 feet in height. Vertically oriented, the tunnel spans from the floor of the basement to the ceiling of the building. The tunnel was designed by West Coast Research Co., of Los Angeles, California in 1955. Under construction from 1955 through 1961, the Academic Wind Tunnel was not operational until 1965. Figure 1.1 is a side view of the facility.

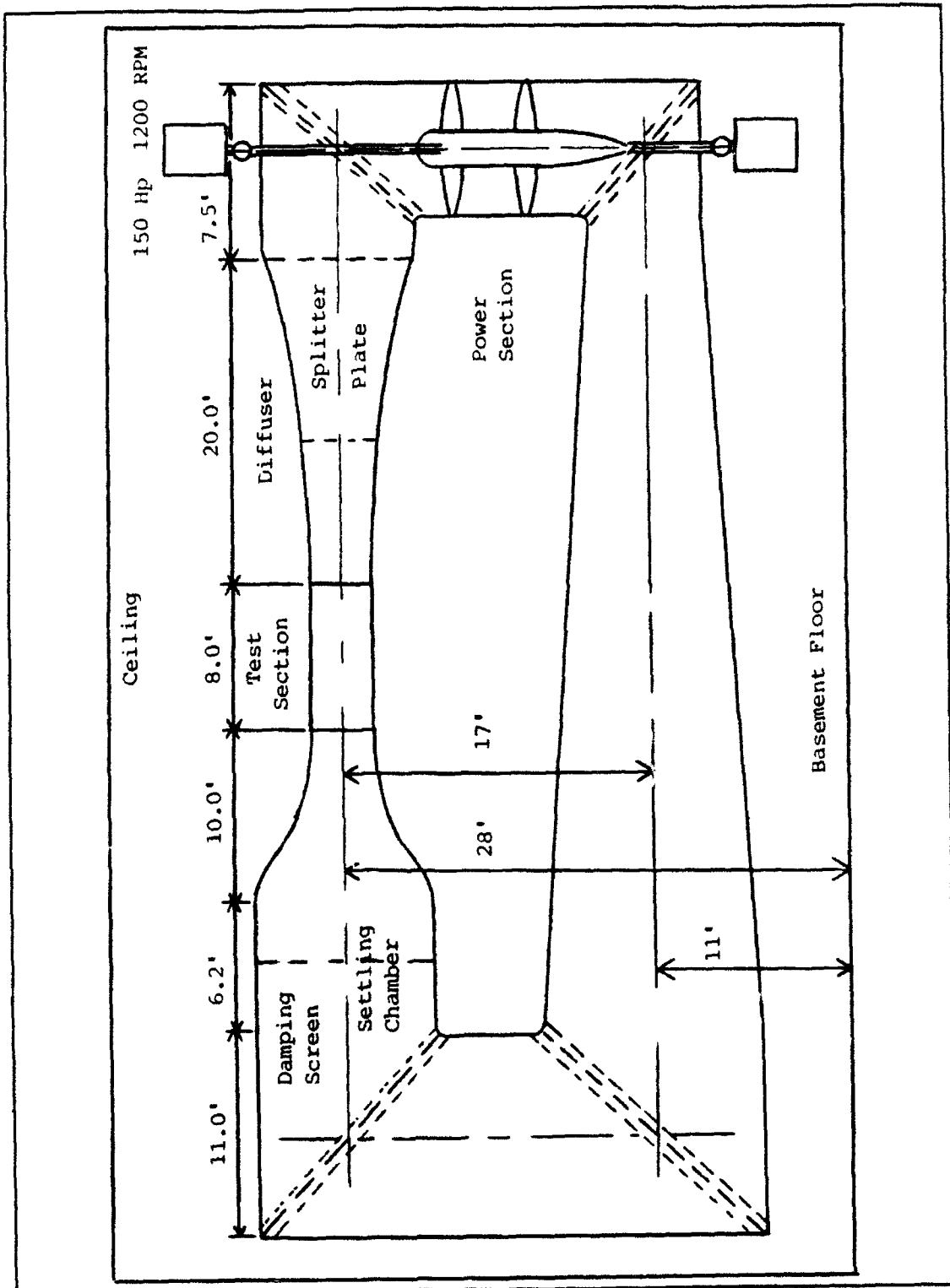


Figure 1.1 Academic Wind Tunnel

During designed 200-knot operations, two 150-horsepower electric motors power two four-blade counter-rotating propellers. The tunnel does not incorporate flow straighteners following the power section since the dual propeller system was designed to remove swirl at all blade pitch angles and tunnel speeds. Turning vanes with adjustable trailing edge tabs are located at each corner of the tunnel. The settling chamber provides a contraction ratio of 6.9 and is an ideal location to place screens and other devices which reduce turbulence and provide a uniform airstream into the test section. A breather slot is located at the exit of the test section and is used to exchange air with the tunnel room during tunnel start and stop conditions. An equally important breather slot function is to maintain a uniform pressure in the test section relative to atmospheric pressure by supplementing airflow leakage losses which occur throughout the tunnel circuitry. The eight-foot-long test section is octagonal in shape and offers visual and physical access from both sides of the tunnel. The side walls are hinged at the top and open outward to expose the entire length of the test section.

Unfortunately, the tunnel has not operated at design conditions since the early 1980's. A screwdriver left inside the test section passed through and damaged the power section of the tunnel. To minimize cost and return the tunnel to operating condition, four of the least damaged blades were

installed on the lower hub assembly. This single fan system reduced maximum speed to 145 knots through the test section. Even in its impaired condition, laboratory experiments and graduate-level research were conducted in the tunnel.

In 1990, Lieutenant Duanne E. Nestor attempted to revitalize the Academic Wind Tunnel. He designed and implemented a digital data acquisition system, performed an airspeed calibration and conducted hot wire experiments to determine turbulence intensity levels. He concluded that turbulence levels of 0.4% could be reduced to 0.3% by installation of a damping screen in the settling chamber.

[Ref. 1:p. 46]

B. THE MODIFICATION

Following the recommendation of Lieutenant Nestor and Professor Louis V. Schmidt, a fine mesh screen was installed in the settling chamber during February, 1992. The function of such a screen is described in Pankhurst and Holder [Ref. 2:p. 28].

The physical explanation of the action of such a screen is that large scale eddies are removed at the expense of the introduction of a larger number of eddies of much smaller scale which are found to decay rapidly. The screen thus decreases the turbulence at a sufficient distance downstream although it may considerably increase the turbulence at small distances.

Screens made of small diameter wire placed in the low-speed region upstream of the contraction cone, could reduce the

level of turbulence in the test section.

The settling chamber is 10.0 feet wide and 10.0 feet high. The screen material used was 16 mesh stainless steel wire which came in four-foot-wide rolls. To provide a uniform screen across the entire area, the rolls of screen were laid out vertically with a center section four feet wide and a three-foot-wide section on either side. The screen was located 13.5 feet upstream of the entrance to the test section and experienced a slight axial sag as a result of stresses associated with aerodynamic loads.

The drop in pressure due to the presence of the damping screen was calculated using the procedures in Appendix A of Pankhurst and Holders' text.

$$K = \frac{P_1 - P_2}{1/2\rho V_1^2} \quad 1.1$$

where p_1 and p_2 are the pressures upstream and downstream of the screen respectively, ρ is the density of the fluid, V_1 is the upstream velocity and K is the resistance coefficient. From standard gauze data tables and Figure 370 in Appendix A, 16 mesh screens with wire diameters of 0.009 of an inch are predicted to have a resistance coefficient equal to 0.7. This conclusion was based on a Reynolds number with the velocity equal to 30.0 ft/sec. This equated to a theoretical pressure drop of 0.75 lb_f/ft² across the damping screen. [Ref. 2]

C. WIND TUNNEL CALIBRATION

Determination of flow characteristics through the test section is required before conducting operational and experimental research. These procedures must be performed following tunnel construction and any time the tunnel is modified. Meaningful experimental results can only be obtained if the approaching airstream is well defined. For low speed wind tunnels, the airstream is defined when the distribution of dynamic pressure, static pressure, and total pressure are known along with the tunnel temperature and turbulence [Ref. 3:p. 85].

The tunnel calibration process is broken down into five phases.

- Lateral Pressure Variation. Flow measurement devices are traversed laterally across the test section to ensure a uniform pressure and velocity distribution.
- Longitudinal Pressure Variation. Flow measurement devices are utilized to measure the static pressure gradient from the entrance cone to the exit cone of the test section. This test is necessary if buoyancy corrections are to be made.
- Flow Angularity. Measurements using multiple port pressure sensing devices identify the presence of swirl or rotation of the airflow through the test section. If excessive or unknown amounts of swirl exist, errors in all force and moment calculations will be induced.
- Tunnel Turbulence Level. Pressure or electrical measuring devices are utilized to ensure the results of wind tunnel testing may be applied to the conditions of free flight. Excessive turbulence levels dramatically alter the effective Reynolds number which could invalidate the results.

- Test Section Airspeed. Flow velocity through the test section is regulated by a reference pressure differential. These pressure sensing devices are located upstream of the test section well away from the tunnel centerline. If dimensionless performance parameters are to be accurately calculated, the actual velocity along the centerline must be known.

Paragraph 3.0 of the "General Specifications for the 3.5 ft. X 5.0 ft. - 200 knot Academic Wind Tunnel" directed performance specifications which would be used as acceptance criteria following tunnel construction. Specifically, deviation from mean design velocity across the test section was limited to less than 1.0%. A static pressure variation of approximately 1.0% of the mean dynamic pressure along the longitudinal axis was permitted. Angularity of flow was to be within 0.5° with respect to the axis of the test section. The turbulence level without screens was to be within 1.0% parallel and 1.5% perpendicular to the flow in the test section. [Ref. 4]

In 1959, the Navy Department terminated its contract with the West Coast Research Co. after the Academic Wind Tunnel had fallen three years behind the construction schedule, exceeded cost estimates and failed its acceptance calibration. Excessive power required to generate the maximum tunnel velocity of 200 knots, large changes in temperature during runs, high turbulence levels and poor construction methods were cited in the ensuing lawsuit. The project was turned over to the TASK Corporation of Anaheim, California. They

repaired numerous pressure leaks and improved flow angularity by adjustment of the trailing edge tabs on the turning vanes. Over the years, fine tuning of the tunnel has been performed by personnel within the Department of Aeronautics and Astronautics.

II. EXPERIMENTAL PROCEDURES

For ease of visualization, Figure 2.1 contains a side and cross-sectional view of the test section. With the viewer facing upstream, the tunnel wall to the left was designated position "0" and the right wall was labelled position "60". All flow measurements were taken on the vertical centerplane, 21.0 inches above the tunnel floor. The position of the reference pitot and ring static system used to set the tunnel dynamic pressure (q) in the test section is included in Figure 2.1.

Unless otherwise indicated all traversing gear, mounting equipment and measuring devices were designed by the author and built by Naval Postgraduate School technicians.

A. LATERAL PRESSURE MEASUREMENTS

Mounting hardware for a lateral traversing system already existed on the side walls of the test section. The support assembly was located 15.0 inches above the tunnel floor and 28.0 inches aft of the entry to the test section. Various pressure sensing devices could be attached to a cylindrical pole and traversed across the tunnel. An 11.0-foot-long stainless steel pole was located and used for this purpose. Circular rings were etched every inch along the pole in order to mark the lateral position of the probe in the test section.

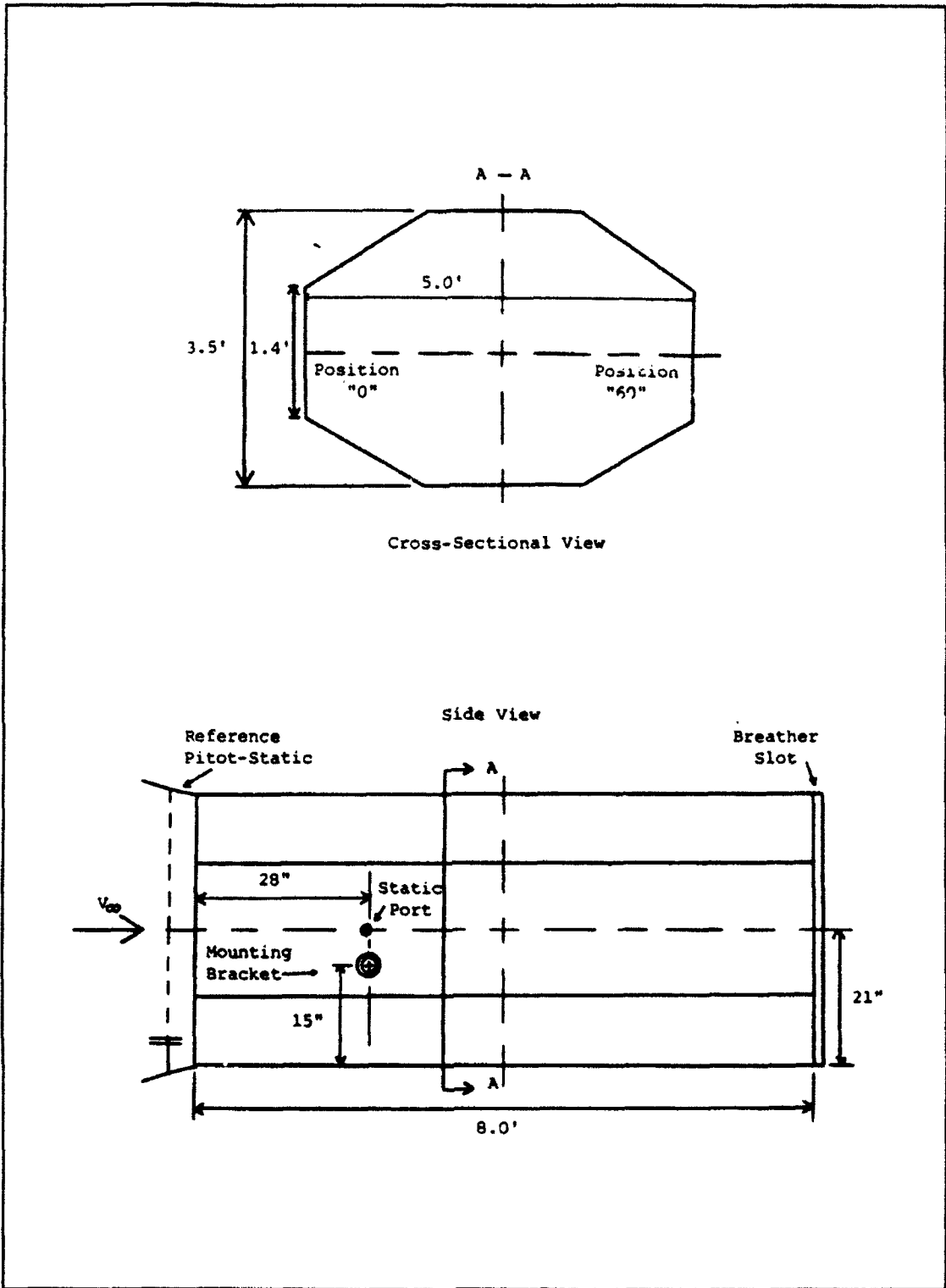


Figure 2.1 Test Section Schematic

A single longitudinal line was etched along the pole to be used as a witness mark to maintain probe alignment with the airstream. A reference witness mark was etched on the mounting support assembly.

In uniform flow a pitot-static probe is used to measure stagnation or total pressure (p_o) and static pressure (p_∞). With these values the tunnel dynamic pressure (q) is determined using the Bernoulli equation. For incompressible low-speed flows this reduces to

$$q = p_o - p_\infty = 1/2\rho V_\infty^2. \quad 2.1$$

A Kiel probe was used to measure total pressure across the test section. This device was chosen for its unimpaired accuracy over a range of yaw angles. Dimensions for the Kiel probe were scaled from Figure 7-41 in Holman [Ref. 5]. Figure 2.2 is a photograph of the Kiel probe in the test section.

Static pressure measurements in a flowstream of uncertain direction are considerably more difficult than those of total pressure. The most accurate way to measure static pressure under these conditions was to measure the static pressure at the wall where the flow direction was confined. To account for local flow perturbations, the reference static ring consisted of five ports which averaged the static pressure along the wall. Since the reference static ring was not located in the test section, a static port was designed and



Figure 2.2 Kiel Probe and Static Pressure Port

located on the vertical centerplane at position "60". The divergent side walls of the test section provided a challenge to mount the static port flush. The static pressure read from this port was equal to the averaged static pressure of the reference ring at all tunnel speeds. This provided an accurate measurement of static pressure along the lateral path of the traversing probes. The static port is visible in Figure 2.2.

A static pressure probe was designed and used to provide a knowledge of the static pressure variation across the test section. If the flow angularity proved to be within acceptable limits, the static pressure readings could be combined with the total pressure readings to determine the lateral variation in dynamic pressure. Figure 2.3 is a photograph of the static pressure probe in the test section.

1. Data Acquisition

A mounting bracket was designed to attach both probes to the traversing pole. Tygon tubing was run from the probes through the center of the pole and out to a wall manometer. Since readings were taken visually from the wall manometer, they were deemed accurate to within ± 0.1 inches of water.



Figure 2.3 Static Pressure Probe

Conversion of the data from heights of water to pressure followed the relationship

$$1 \text{ ATM} = 406.96 \text{ inches } H_2O = 2116.2 \text{ lb}_f/\text{ft}^2. \quad 2.2$$

B. LONGITUDINAL PRESSURE MEASUREMENTS

Before beginning this phase of the calibration, a thorough investigation of the tunnel was conducted. Several locations allowing pressure losses were discovered in the settling chamber and at the entrance to the test section. The port side of the breather slot was gently taking in air from the tunnel room while the starboard side was pulsing air out at a higher rate. Additionally, fluctuations in total pressure were observed while trying to establish a constant dynamic pressure.

The computer system which enhanced data acquisition for the Academic Wind Tunnel was being used for an experiment in the Aerolab Wind Tunnel. Without it, a time history of the pressure oscillations could not be accurately recorded and analyzed. The decision was made to postpone this experiment until the data acquisition system was available.

C. FLOW ANGULARITY

"Though many wind tunnels exhibit an angular variation of ± 0.75 deg or even ± 1.0 deg, it is not believed that accurate

testing can be done with a variation greater than ± 0.50 deg." [Ref. 3:p. 112] The West Coast Research Co., temporarily placed two heavy damping screens in the settling chamber and used a dual slotted, cylindrical flow inclination probe to claim compliance with the 0.5° angularity performance specification. Since that time, several flow angularity measurements have been conducted. The most recent data was compiled by Captain Christopher L. Sargent, United States Army, in 1985. He examined the flow angularity of the Academic Wind Tunnel prior to investigating the influence of helicopter tail shapes on drag [Ref. 6]. Results of his data are presented for comparison in Chapter III.

The yawhead probe used for flow angularity measurements was designed by Professor Louis V. Schmidt in March, 1965. The probe consisted of five ports which were drilled in a hemispherical nose $13/16$ inch in diameter. One port was aligned with the axis of the yawhead. The remaining four ports were equally spaced and concentrically arranged around the center port. Pressure leads were internally routed through the 7.25 inch sting mount. In practice, the alignment of the yawhead was adjusted until pressures on opposite sides of the center port were equal. When this occurred, the probe was aligned with the direction of the flow. Figure 2.4 is a photograph of the yawhead attached to the three strut balance.

This yawmeter takes advantage of the known flow properties about a sphere. The Coefficient of Pressure (C_p) is defined



Figure 2.4 Yawhead Probe

as

$$C_p = \frac{p - p_\infty}{q_\infty} . \quad 2.3$$

The application of Bernoulli's equation

$$p_\infty + 1/2\rho V_\infty^2 = p + 1/2\rho V^2 \quad 2.4$$

reduces the numerator to

$$p - p_\infty = 1/2\rho (V_\infty^2 - V^2) . \quad 2.5$$

Now the Coefficient of Pressure is defined as

$$C_p = \frac{1/2\rho (V_\infty^2 - V^2)}{1/2\rho V_\infty^2} = 1 - \left(\frac{V}{V_\infty}\right)^2 . \quad 2.6$$

For flow about a sphere [Ref. 7:p. 383]

$$V_\theta = 3/2V_\infty \sin\theta \quad 2.7$$

which when substituted into Equation 2.6 yields

$$C_p = 1 - 9/4\sin^2\theta \quad 2.8$$

or equivalently

$$p - p_{\infty} = q_{\infty}(1 - 9/4\sin^2\theta). \quad 2.9$$

Figure 2.5 is a schematic of the yawhead at some flow inclination (α). For flows aligned off axis the following three equations determine the pressure differential due to the flow inclination:

$$p_{\theta 5} - p_{\infty} = q_{\infty}(1 - 9/4\sin^2\alpha) \quad 2.10$$

$$p_{\theta 1} - p_{\infty} = q_{\infty}(1 - 9/4\sin^2(\alpha + \theta)) \quad 2.11$$

$$p_{\theta 3} - p_{\infty} = q_{\infty}(1 - 9/4\sin^2(\alpha - \theta)). \quad 2.12$$

If

$$\Delta p_{\theta} = p_{\theta 1} - p_{\theta 3} \quad 2.13$$

then

$$\Delta p_{\theta} = 9/4q_{\infty}(\sin^2(\alpha - \theta) - \sin^2(\alpha + \theta)). \quad 2.14$$

Using the following trigonometric identities

$$\sin^2(\theta) = 1/2(1 - \cos 2\theta) \quad 2.15$$

and

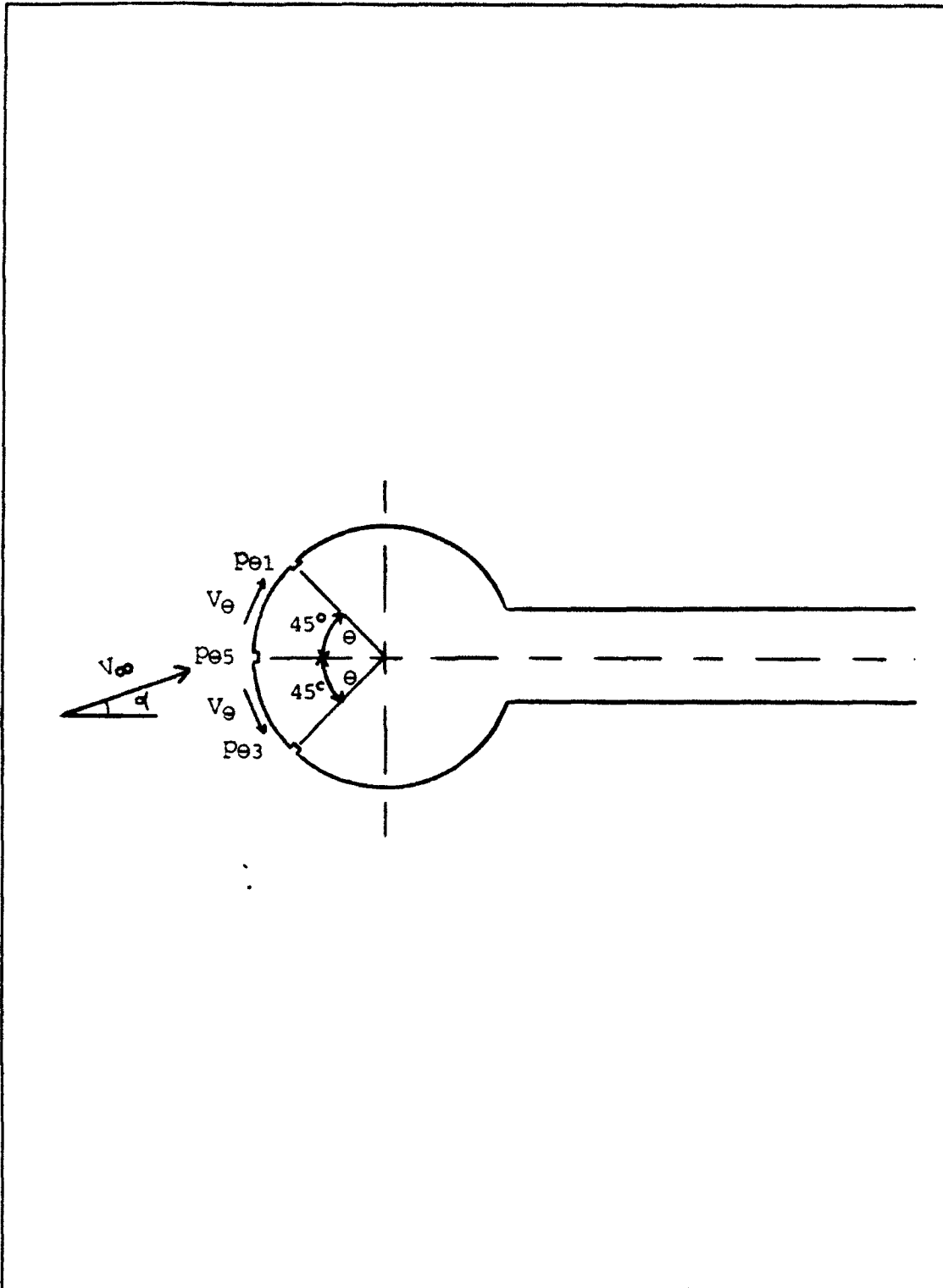


Figure 2.5 Yawhead Description

$$\cos(\alpha \pm \theta) = \cos\alpha\cos\theta \mp \sin\alpha\sin\theta \quad 2.16$$

Equation 2.14 reduces to

$$\Delta p_{\theta} = -9/4q_{\infty}(\sin 2\alpha \sin 2\theta). \quad 2.17$$

Non-dimensionalizing with respect to the axis of the probe yields

$$\frac{\Delta p_{\theta}}{p_{\theta 5} - p_{\infty}} = \frac{-9/4 \sin 2\alpha \sin 2\theta}{1 - 9/4 \sin^2 \alpha}. \quad 2.18$$

Using the fact that the "sin2 θ " term in Equation 2.18 is at a maximum value when $\theta=45.0^{\circ}$, the orifice locations on the yawhead were located at the 45.0° position relative to the axis of the probe. This provided theoretical values for the pressure relationship as a function of the flow inclination. With $\theta=45.0^{\circ}$, Equation 2.18 reduces to

$$\frac{\Delta p_{\theta}}{p_{\theta 5} - p_{\infty}} = \frac{-9/4 \sin 2\alpha}{1 - 9/4 \sin^2 \alpha}. \quad 2.19$$

A calibration of the yawhead was performed to establish the actual pressure variation with respect to a known flow inclination, vice the predicted variation of Equation 2.19. The difference in pressure between ports $p_{\theta 1}$ and $p_{\theta 3}$ will be used for an example. The same procedures were used for ports

$p_{\theta 2}$ and $p_{\theta 4}$.

The yawhead probe was calibrated in the wind tunnel using a geometric angle of attack (α_g) referenced to the centerline of the test section. The yawhead was attached to the three strut balance and positioned on tunnel centerline with $p_{\theta 1}$ and $p_{\theta 3}$ vertically aligned with $p_{\theta 5}$. Zero α_g was established with a carpenter level using the axis of the sting mount as a horizontal reference. Subsequent angles of inclination were controlled and monitored with a remote indicating angle of attack sensing unit. This system provided an electrical signal output and is described in Nestor [Ref. 1]. Pressure readings for $p_{\theta 1}$, $p_{\theta 3}$ and $p_{\theta 5}$ were taken for geometric angles of attack from 20° down (-20°) to 20° up ($+20^\circ$). The probe was then inverted and the same measurements were taken again. When plotted as in Figure 2.6, the following information can be obtained.

- The average of the normal and inverted values for pressure on the surface of the sphere was used to determine the relationship with the geometric angle of attack .
- The intersection of the mean line with the horizontal axis denoted the flow inclination angle.
- The difference between the mean line and each plotted line represented the instrument error.

The yawhead was rotated 90.0° and the same procedures were used for $p_{\theta 2}$ and $p_{\theta 4}$. This gave the yawhead the capability to measure both flow alpha and beta angles.

Figures 2.7 and 2.8 are the results of the calibration

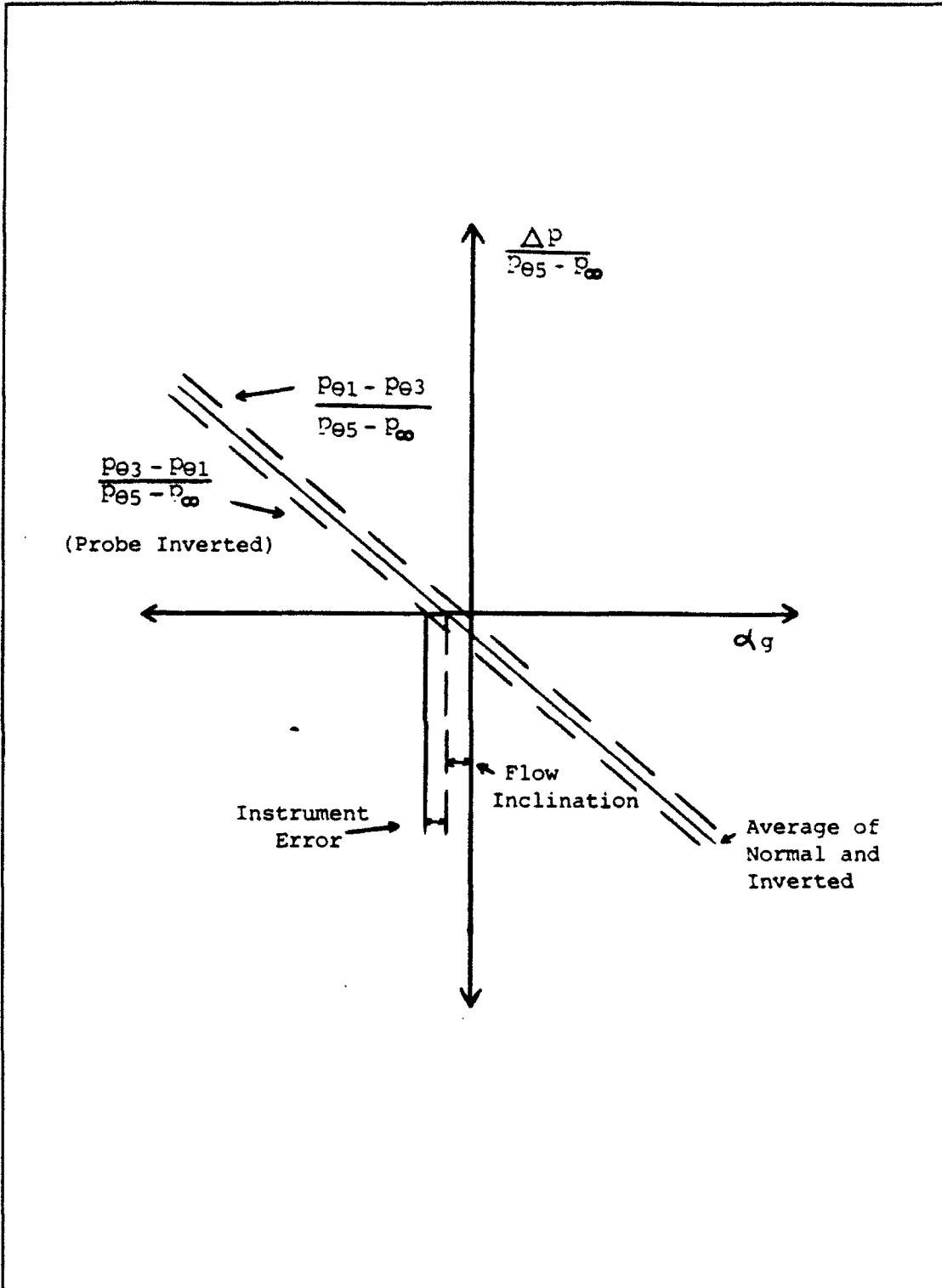


Figure 2.6 Yawhead Calibration Information

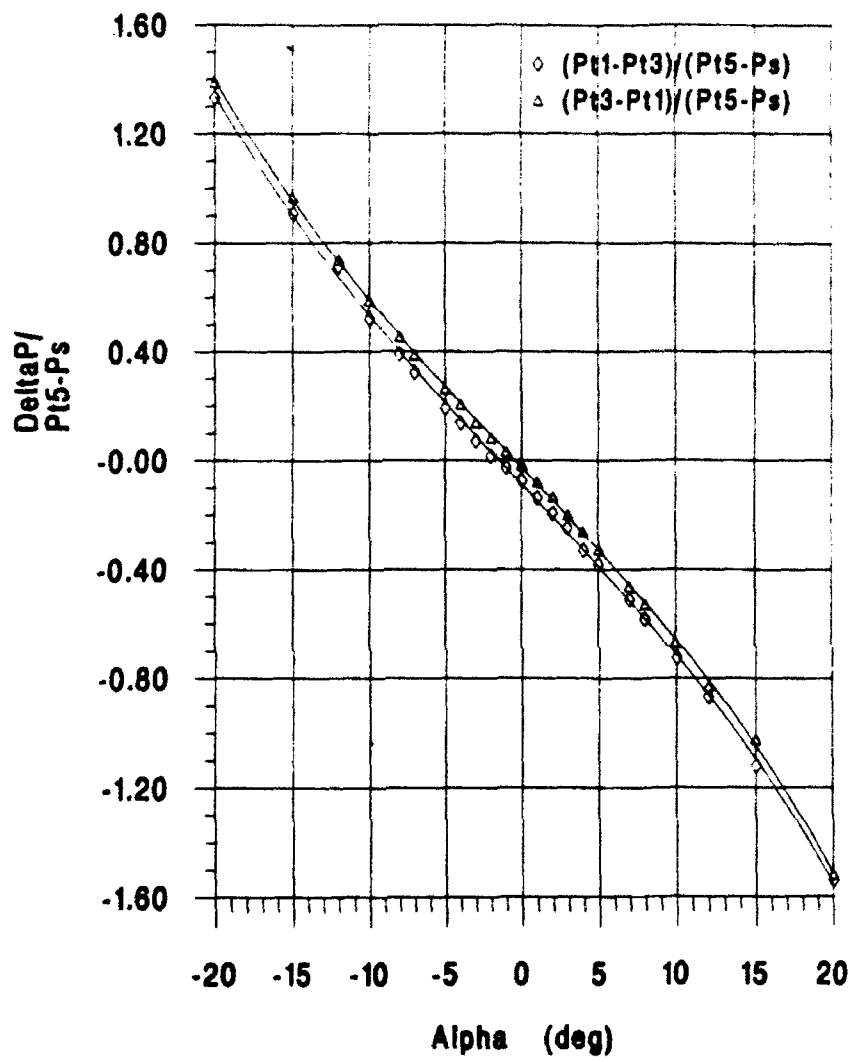


Figure 2.7 $P_{\theta 1}$ and $P_{\theta 3}$ Calibration Results $30 \text{ lb}_f/\text{ft}^2$

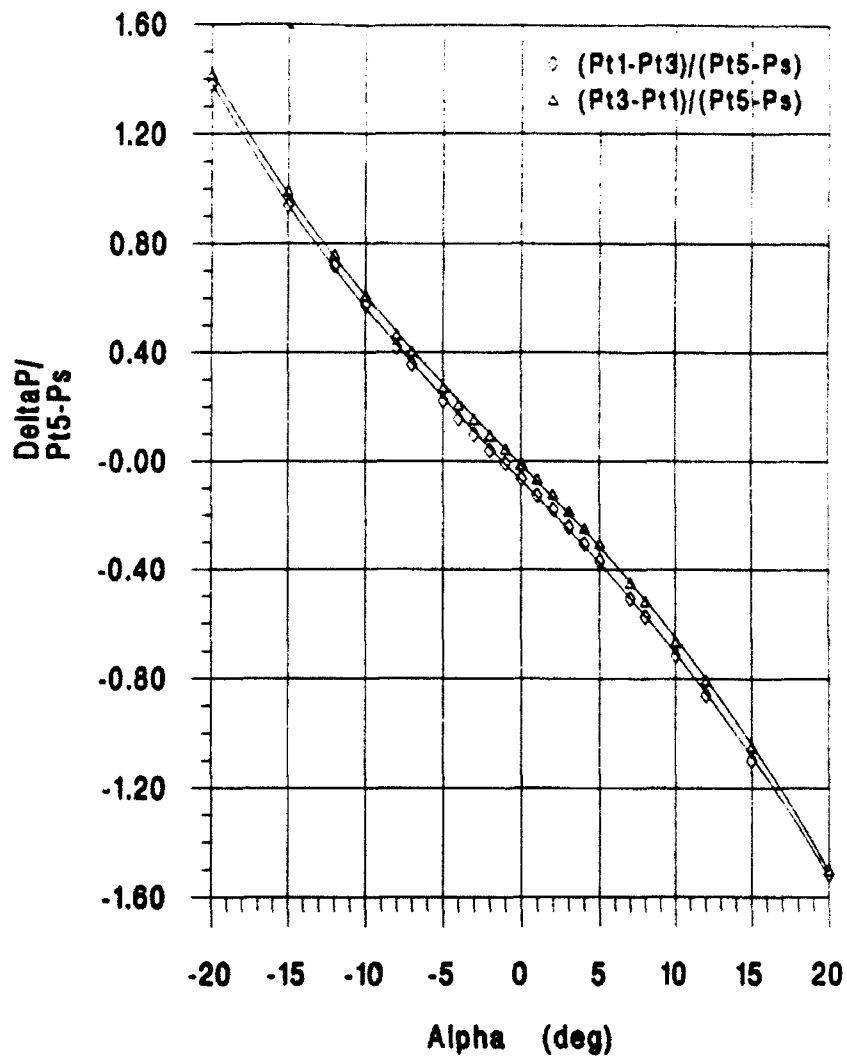


Figure 2.8 P_{01} and P_{03} Calibration Results $50 \text{ lb}_f/\text{ft}^2$

runs for $p_{\theta 1}$ and $p_{\theta 3}$ at dynamic pressures of $30.0 \text{ lb}_f/\text{ft}^2$ and $50.0 \text{ lb}_f/\text{ft}^2$ respectively. Figures 2.9 and 2.10 show the calibration results for $p_{\theta 2}$ and $p_{\theta 4}$ at the same conditions. Figures 2.11, 2.12, 2.13 and 2.14 show these pressure relationships for angle of attack values that would most likely be encountered in the wind tunnel test section. A linear relationship was assumed for this region and the figures revealed a flow inclination angle on tunnel centerline of -1.0° . This translated to a 1.0° upward flow inclination in the test section. The figures also show an instrument error of $\pm 0.02 \text{ deg}^{-1}$.

Once the probe was calibrated, it was secured to a mounting probe and attached to the traversing pole. The yawhead was used to measure flow angularity across the test section by recording the pressure differentials and reading the corresponding angle of attack values from Figures 2.11 through 2.14.

1. Data Acquisition

Tygon tubing connected the yawhead pressure ports $p_{\theta 1}$ through $p_{\theta 4}$ to a wall manometer. Water heights with a ± 0.1 inch accuracy were recorded visually and converted to units of pressure using Equation 2.2. Tygon tubing connected port $p_{\theta 5}$ and the reference static ring (p_w) to a U-tube manometer filled with alcohol. Conversion of the data from height of

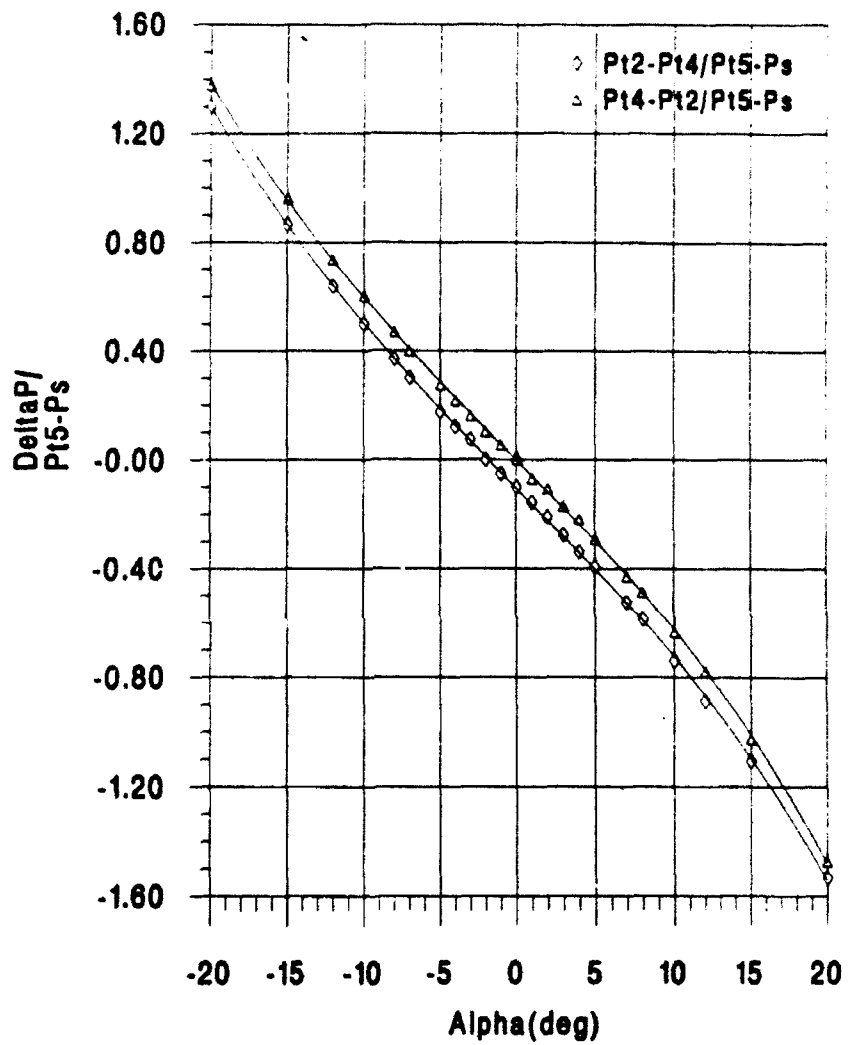


Figure 2.9 $P_{\theta 2}$ and $P_{\theta 4}$ Calibration Results 30 lb_f/ft²

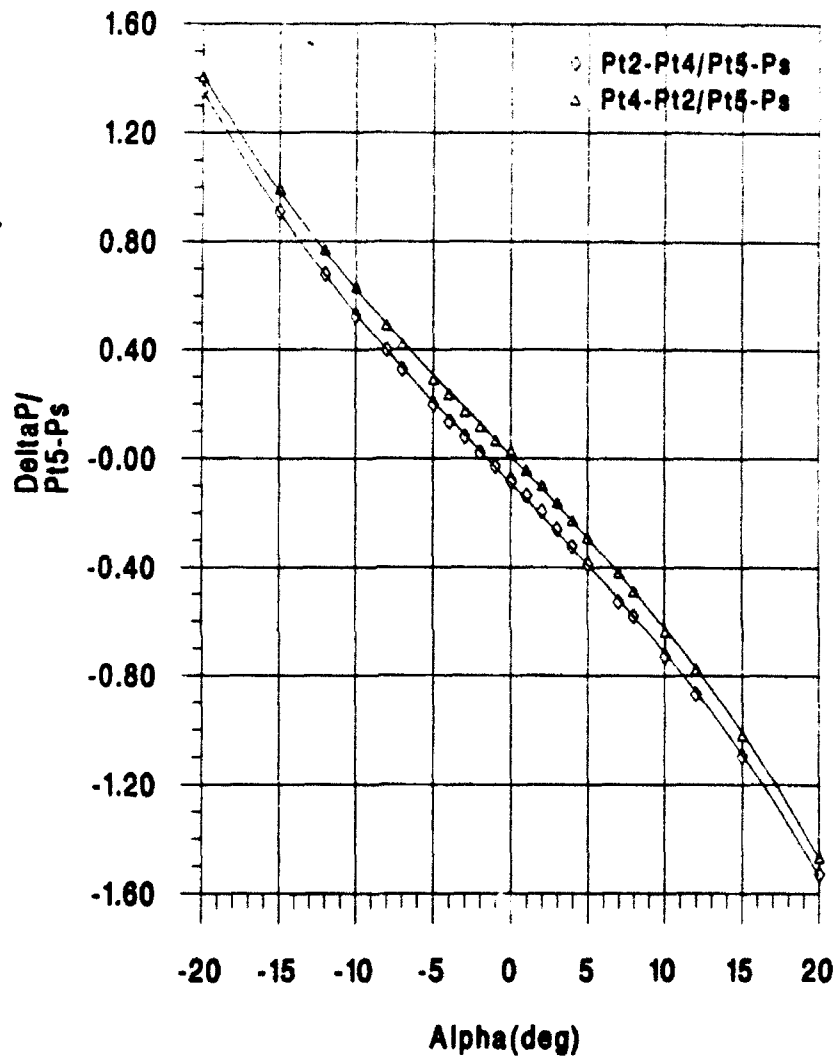


Figure 2.10 $P_{\theta 2}$ and $P_{\theta 4}$ Calibration Results $50 \text{ lb}_f/\text{ft}^2$

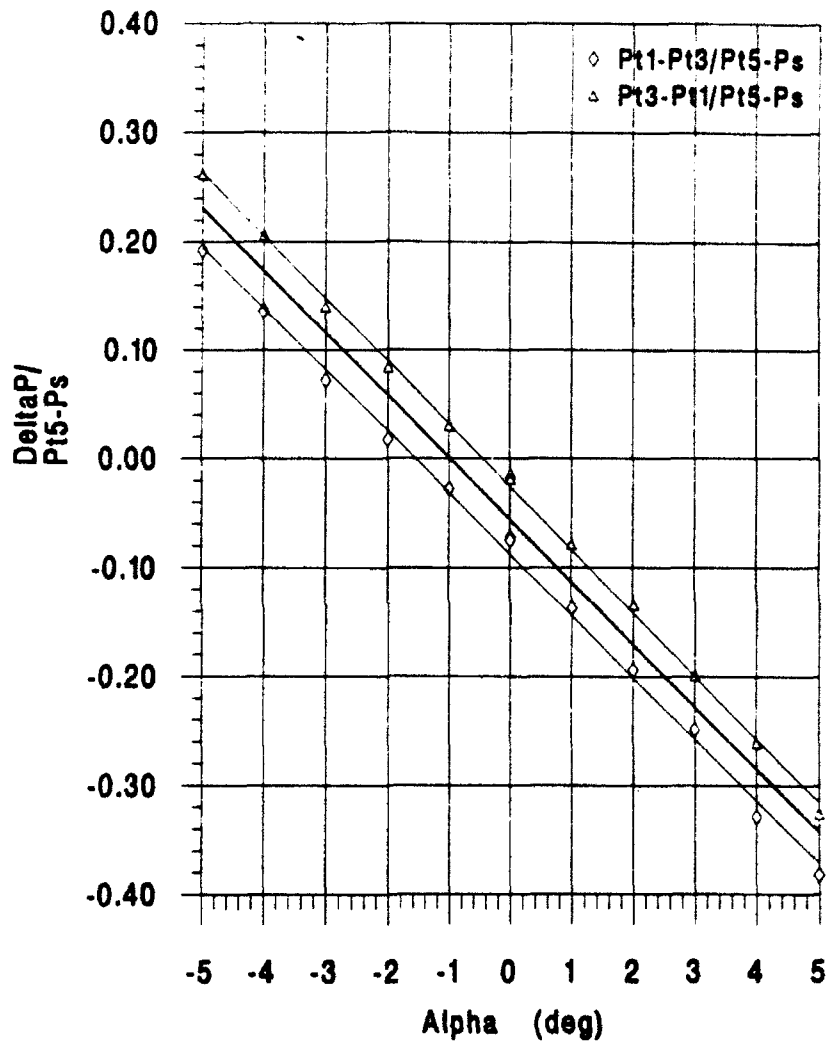


Figure 2.11 P_{θ_1} and P_{θ_3} Results of Interest $30 \text{ lb}_f/\text{ft}^2$

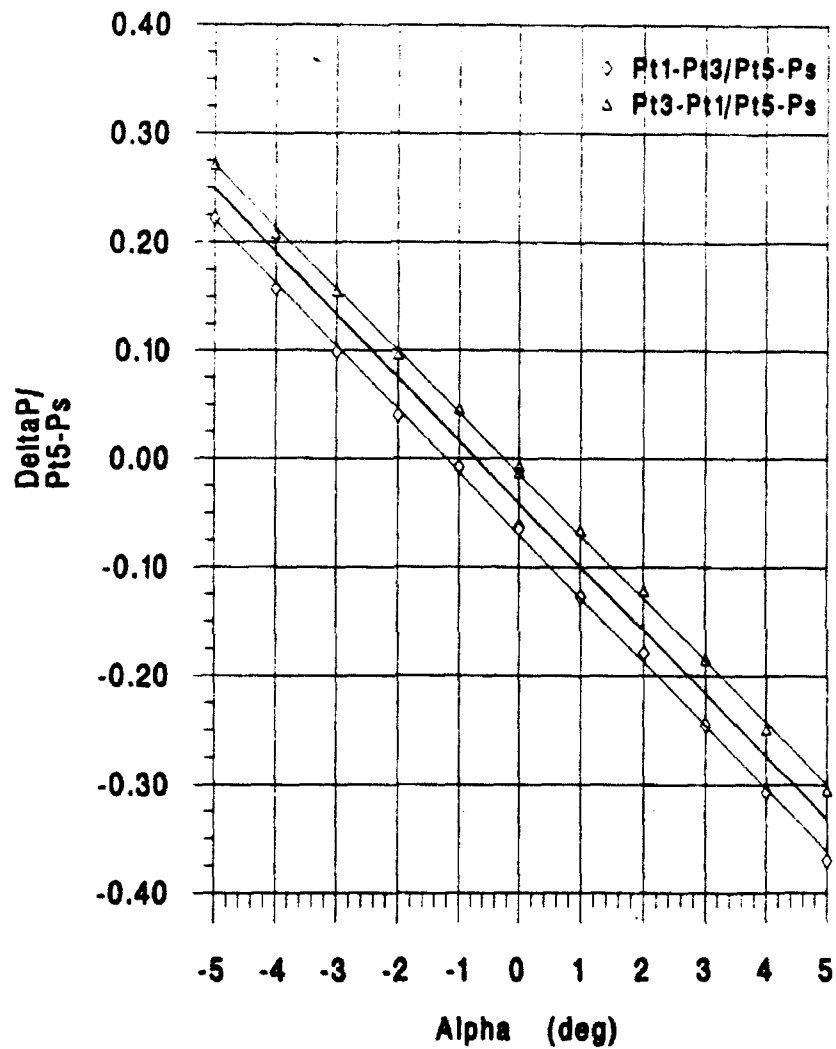


Figure 2.12 $P_{\theta 1}$ and $P_{\theta 3}$ Results of Interest $50 \text{ lb}_f/\text{ft}^2$

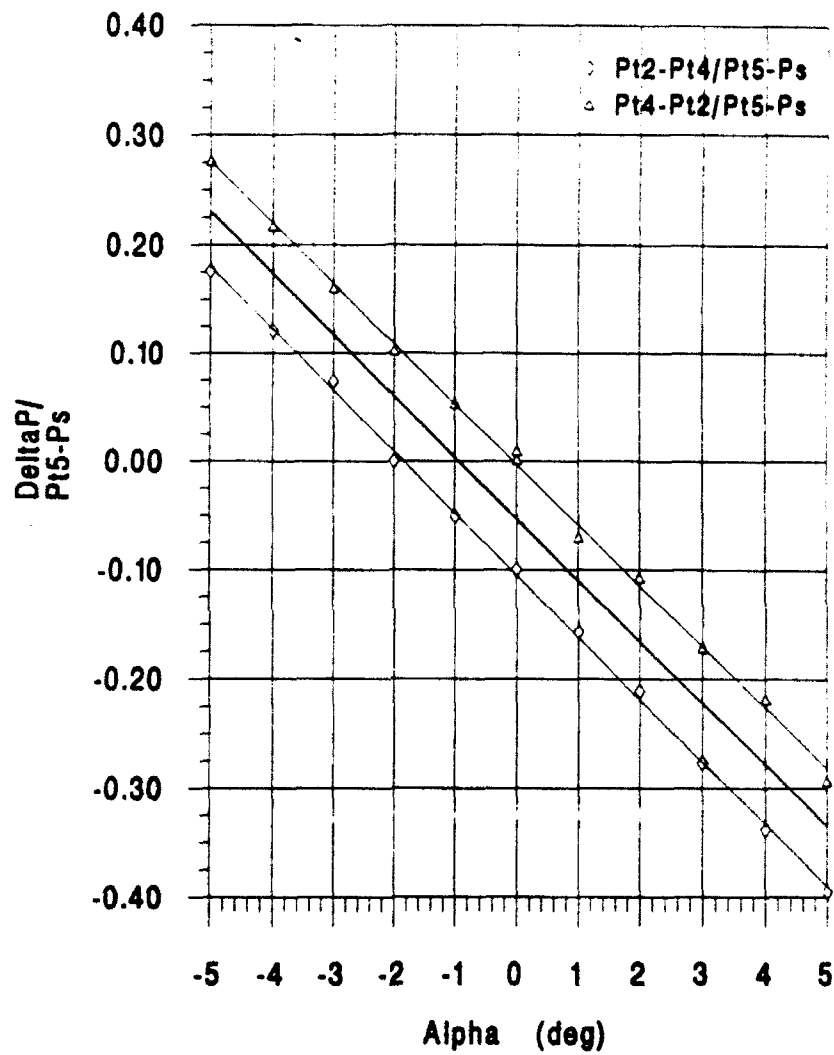


Figure 2.13 $P_{\theta 2}$ and $P_{\theta 4}$ Results of Interest $30 \text{ lb}_f/\text{ft}^2$

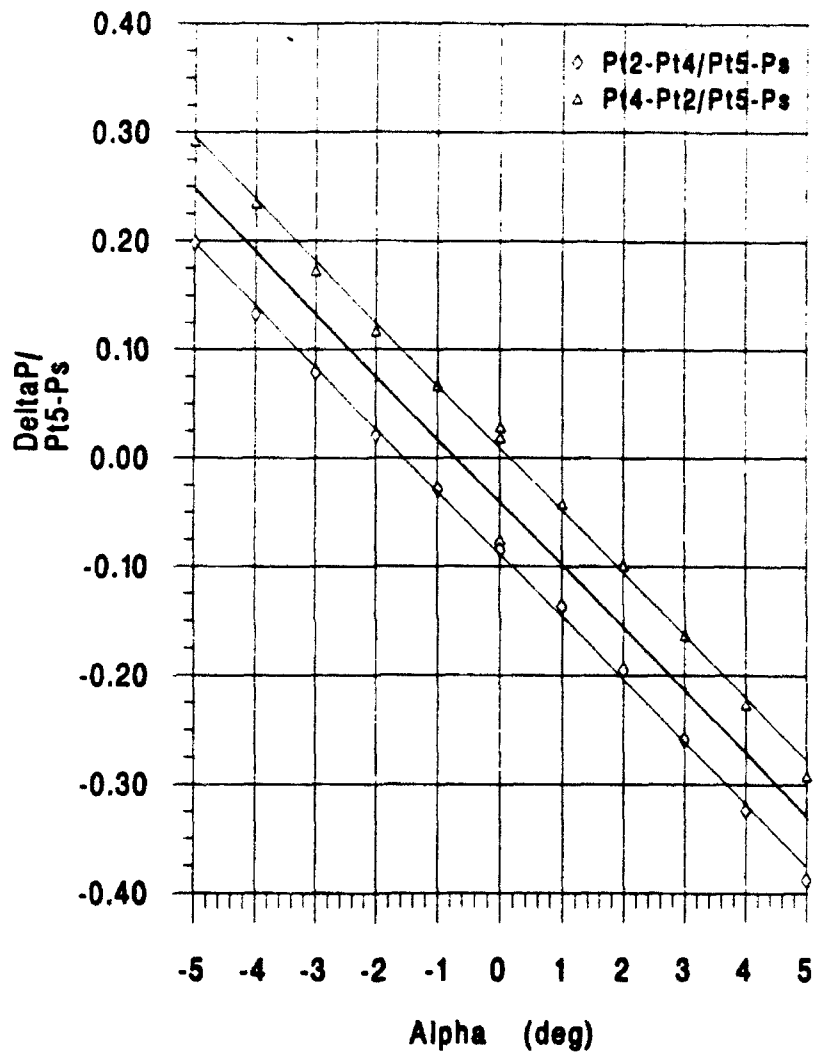


Figure 2.14 P_{θ_2} and P_{θ_4} Results of Interest $50 \text{ lb}_f/\text{ft}^2$

alcohol to units of pressure followed the relationship

$$1 \text{ ATM} = 516.15 \text{ inches alcohol} = 2116.2 \text{ lb}_f/\text{ft}^2. \quad 2.20$$

Angle of attack settings during calibration were set using a voltmeter and were accurate to $\pm 0.01^\circ$.

D. AIRSPEED CALIBRATION

Once flow direction was determined inside the test section, a pitot-static tube was used to measure the test section dynamic pressure along the tunnel centerline. Figure 2.15 contains a photograph of the pitot-static probe and mounting assembly used during this phase of the calibration. This particular measuring system had been used by previous students in their studies using the Academic Wind Tunnel.

To minimize flow interference the reference pitot-static system was located three inches upstream of the entrance to the test section. This system measured total pressure with a Kiel probe and static pressure with a ring of five flush mounted static ports. It did not measure the dynamic pressure along the centerline of the test section. By inserting a pitot-static probe in this location and concurrently measuring the output of the reference system, the upstream system could be used to establish dynamic pressure in the test section.

A compressibility correction was applied to the readings of the pitot-static calibration system. This correction

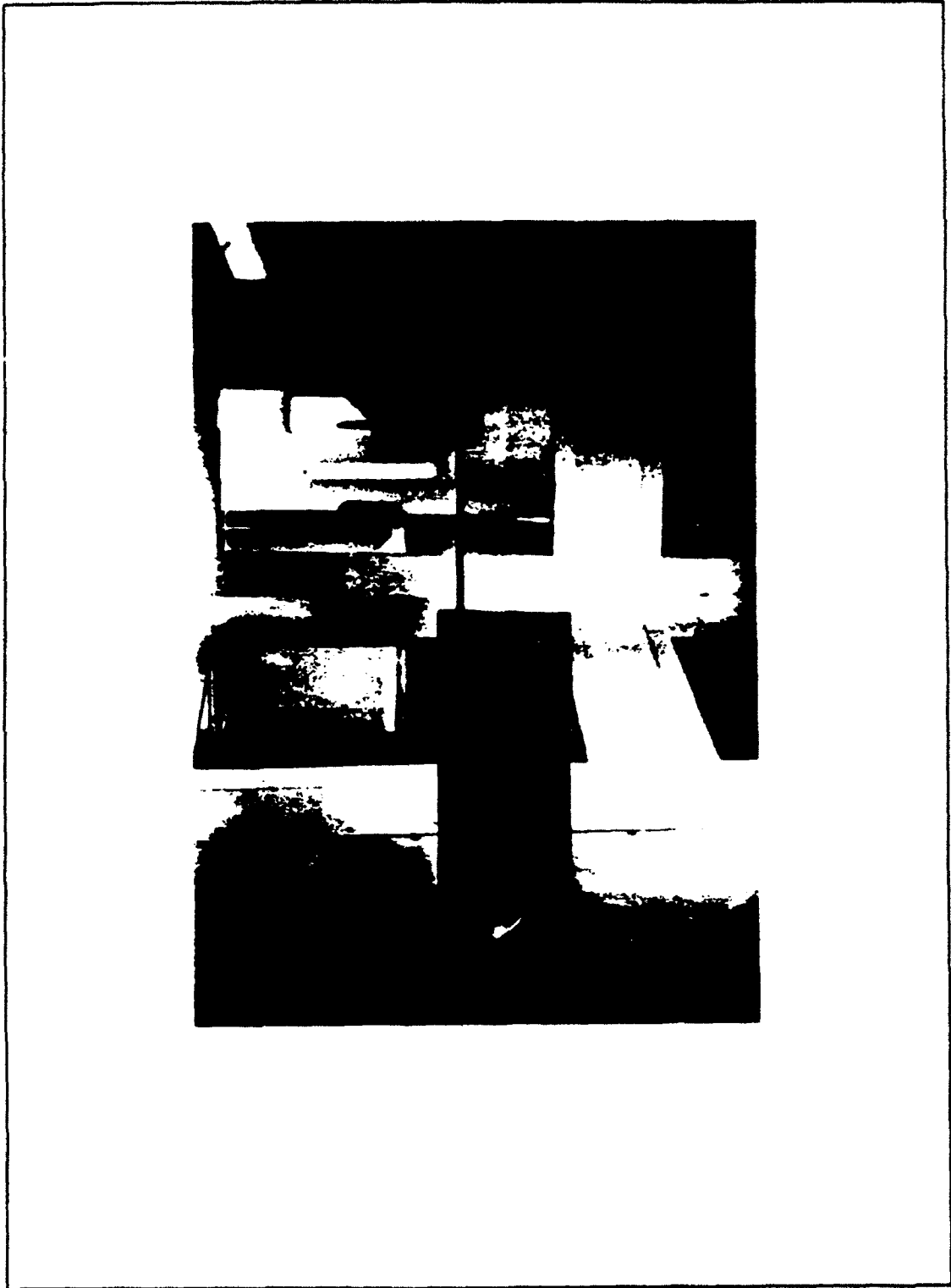


Figure 2.15 Pitot-Static Calibration System

factor is based on the isentropic perfect gas relations for compressible flow and following a binomial expansion results in

$$\frac{P_o - P_\infty}{q} = \left(1 + \frac{M^2}{4} + \frac{(2 - \gamma)M^4}{24} + \dots\right). \quad 2.21$$

Nestor [Ref. 1] discusses the derivation of the compressibility correction. Equation 2.21 was used to correct the measured pressure differential of the calibration system for the often neglected low-speed compressibility effects.

1. Data Acquisition

Tygon tubing connected the total and static pressure probes of each system to two side-by-side micromanometers. It should be noted that the tubing connecting the reference system was four times larger in diameter than the tubing used for the calibration system. This had an effect on the difference in frequency response of the measuring systems. One person monitored each manometer to simultaneously record heights of water. Measurements of water height on the micromanometer were accurate to ± 0.01 centimeters of water. These readings were converted to units of pressure using Equation 2.2.

E. TURBULENCE MEASUREMENTS

The primary reason for installing a damping screen inside the wind tunnel was to reduce the level of turbulence in the

test section. Hot-wire and hot-film anemometers were used to measure the turbulence intensity along the centerline of the Academic Wind Tunnel. These electronically-controlled sensors measure fluid velocity by sensing changes in heat transfer. Key to this transformation is the electronic circuitry used to control the sensor. A TSI Incorporated IFA 100 anemometer served this purpose and used a feedback loop to maintain constant temperature at the sensor.

As the velocity increased past the hot-wire anemometer, temperature and the wire resistance (R_w) decreased. This lower voltage condition was sensed by the IFA 100 which increased the current through the sensor to maintain a constant temperature.

The nonlinear relationship between heat transfer and fluid velocity is expressed by King's Law

$$\frac{E^2}{R} = [a + b(\rho U)^n] \cdot (T_w - T_\infty) \quad 2.22$$

where E^2/R is power supplied, ρ is the density of the fluid, a , b and n are constants obtained from the calibration of the sensor, U is the velocity of the fluid, T_w is the sensor temperature and T_∞ is the freestream temperature of the fluid. For incompressible flow conditions, a linearized form of Equation 2.22 is

$$E^2 = A + BU^n \quad 2.23$$

where A is the square of the voltage at zero velocity (E_0^2) and B and n are determined from calibration of the sensor. Traditionally the value used for n has been 0.45 or 0.5, but a more accurate value can be determined from Equation 2.23 by taking the natural log of both sides and rearranging to get

$$\ln(E^2 - E_0^2) = \ln B + n \ln U. \quad 2.24$$

In this linearized form plotting values of $\ln(E^2 - E_0^2)$ as a function of $\ln(U)$ produced values for B and n.

A single probe hot-wire anemometer cannot discern flow direction. However, orientation of the probe allowed axial and vertical velocity components to be measured. This summation of velocity components in vector form is

$$\vec{U} = u\vec{i} + v\vec{j} + w\vec{k}. \quad 2.25$$

For turbulent flows the instantaneous velocity component consists of a mean velocity plus some velocity fluctuation about that mean. In equation form

$$u\vec{i} = \bar{u} + u' \quad 2.26$$

$$w\vec{k} = \bar{w} + w'. \quad 2.27$$

Figure 2.16 is an illustration of the relationship between mean velocity and the fluctuations about that mean expressed

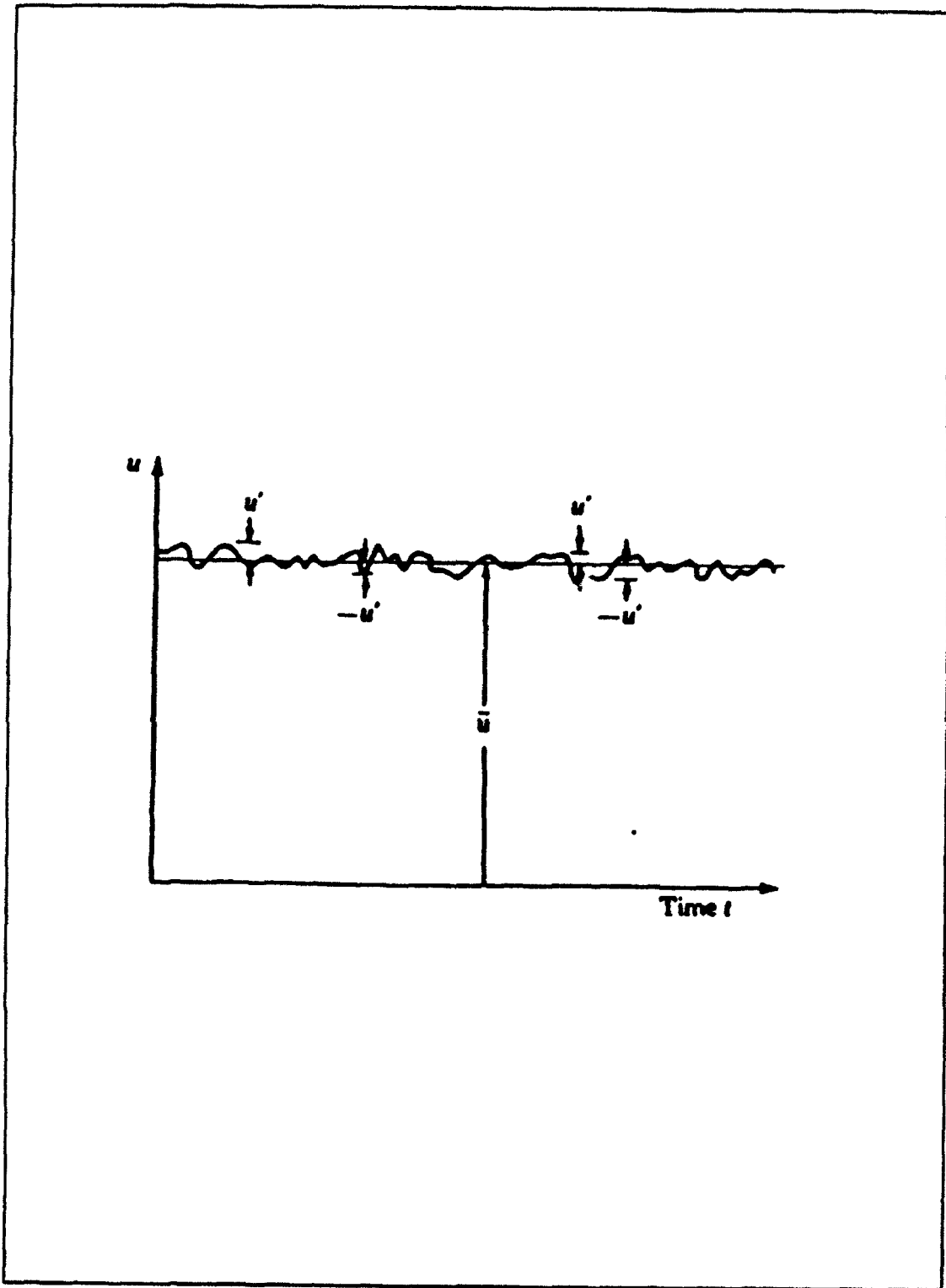


Figure 2.16 Turbulence Fluctuations [Ref. 5:p. 256]

in Equation 2.26. Applying Equations 2.26 and 2.27 to Equation 2.25 produces an expression for the instantaneous velocity

$$\bar{U} = \bar{U} + U' . \quad 2.28$$

Thermal anemometers can respond to very rapid changes in flow velocity. They possess the capability to measure both components of the instantaneous velocity. Substituting Equation 2.28 into Equation 2.23 yields

$$(E + e')^2 = A + B(\bar{U} + U')^2 \quad 2.29$$

where E is the dc voltage required to maintain the sensor at the operating temperature and e' is the rms voltage fluctuations about that mean.

Turbulence intensity is the ratio of the perturbations of the flow velocity to the averaged velocity of the fluid.

$$\text{Turbulence Intensity} = \sqrt{U'^2} / \bar{U} \quad 2.30$$

Rearranging Equation 2.29 yields

$$E^2 + 2Ee' + e'^2 = A + B\bar{U}^n(1 + U'/\bar{U})^n \quad 2.31$$

Expanding the right side of Equation 2.31 with the assumption that $n < 1.0$ yields

$$E^2 + 2Ee' + e'^2 = A + B\bar{U}^n(1 + nU'/\bar{U} + \text{H.O.T.}). \quad 2.32$$

Neglecting the higher order terms and applying Equation 2.23 produces

$$2Ee' = Bn\bar{U}^{(n-1)}U'. \quad 2.33$$

Rearranging and dividing both sides by \bar{U} and realizing the "" values represent rms voltage measurements gives

$$\sqrt{U'^2}/\bar{U} = 2E\sqrt{e'^2}/Bn\bar{U}^n. \quad 2.34$$

Equation 2.34, a linearized version of King's Law, was used to calculate turbulence intensity.

A hot-film and a hot-wire anemometer were used to measure the turbulence intensity within the test section. Hot film sensors are more rugged than hot wires and are normally preferred in flows that contain particle matter which could foul the sensor. Hot wire sensors normally have a higher sensitivity to changes in temperature and offer superior frequency response at minimum noise levels. For future correlation the types of probes used during this phase of the tunnel calibration are listed in TABLE 2.1.

TABLE 2.1 PROBE DESCRIPTION

Probe Type	Material	Diameter	Length
Hot Film Dantec 55P01	Nickel on Quartz Fiber	70 μm	1.25 mm
Hot Wire Dantec 55P11	Plat.-plated Tungsten	5 μm	1.25 mm

Knowledge of turbulence intensity levels over a range of tunnel speeds was desired. Calibration of each sensor was performed in accordance with the procedures contained in Chapters 3 and 4 of the IFA 100 Instruction Manual [Ref. 7]. Figure 2.17 compares the nonlinear relationship between the voltage required to maintain the hot film and the hot wire at 250°C over the range of tunnel velocities. Figures 2.18 and 2.19 show the same information following linearization according to Equation 2.24 for the hot film and hot wire respectively.

1. Data Acquisition

Figure 2.20 is a photograph of the hot wire anemometer probe mounted to the three strut balance. Before proceeding with the calibration, the tunnel temperature was allowed to rise to a level which could be maintained constant during the runs. Rms voltages were recorded at each data point since the data points coincided with the velocities of interest. The mean voltage (E) was read directly from the IFA 100 and the rms voltage ($\sqrt{e'^2}$) was read from a Hewlett Packard 3400A RMS Voltmeter. A Hewlett Packard 1741A Oscilloscope was used to

$$\text{Hot Film } E = 1.2000E+0 + 2.6783E-2U - 1.9462E-4U^2 + 7.6236E-7U^3 - 1.1620E-9U^4$$

$$\text{Hot Wire } E = 9.1801E-1 + 1.3952E-2U - 1.0962E-4U^2 + 4.4084E-7U^3 - 6.7454E-10U^4$$

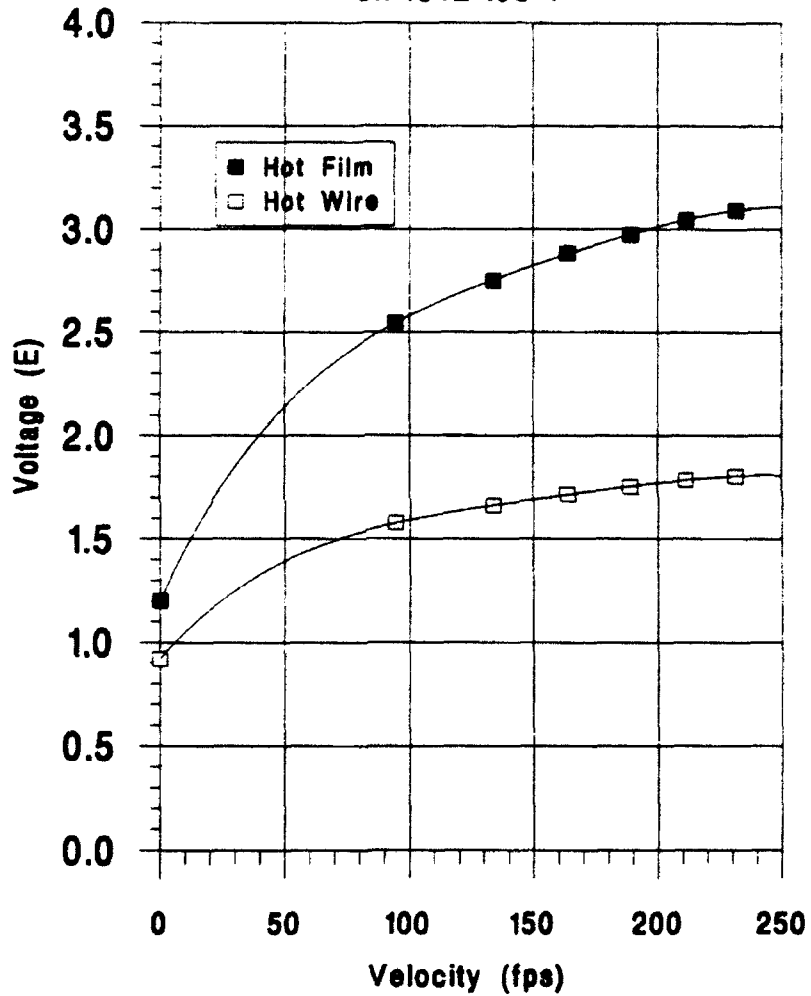


Figure 2.17 Voltage vs Velocity: Hot Wire and Hot Film

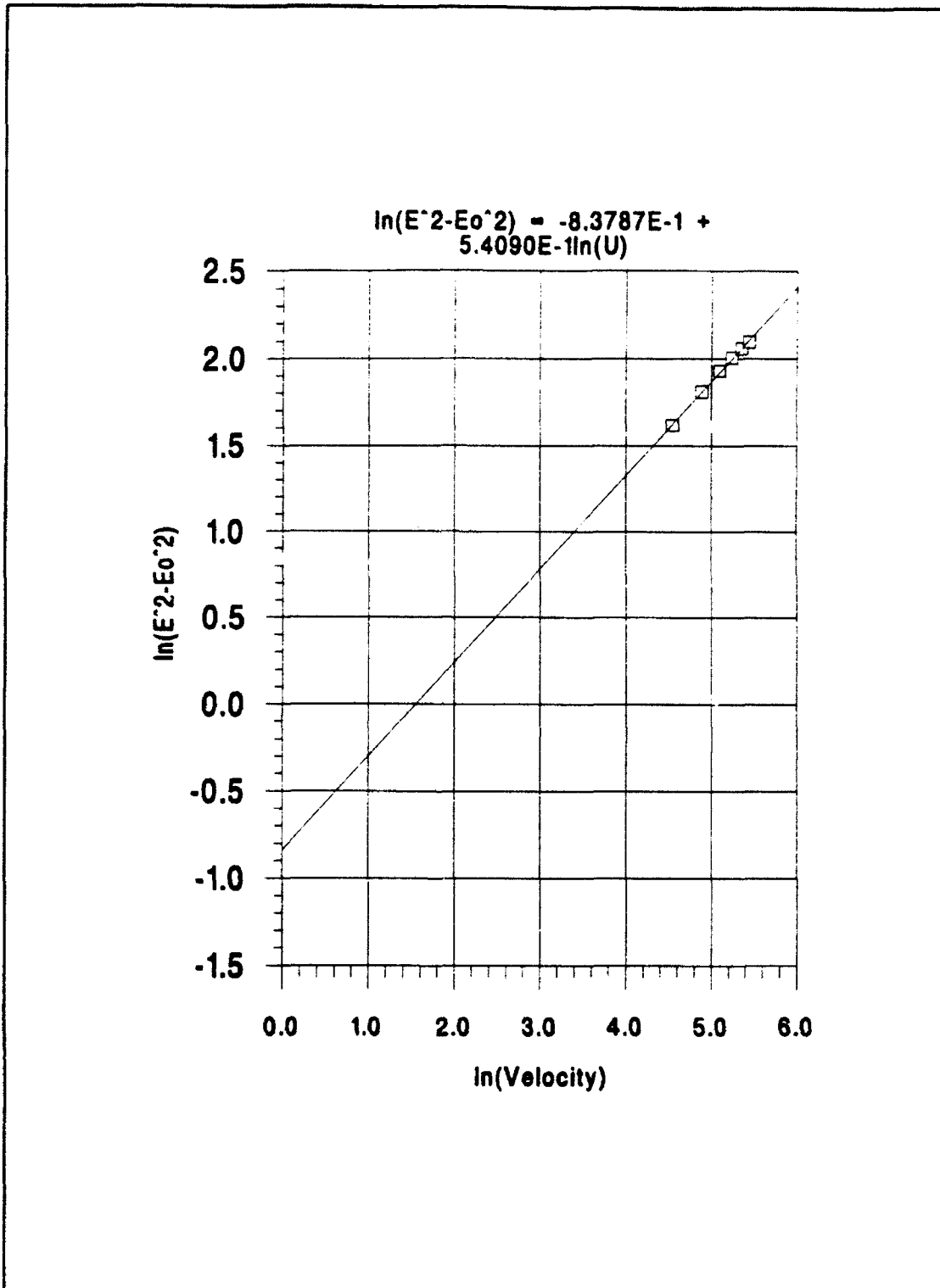


Figure 2.18 Linearized Calibration of Hot Film

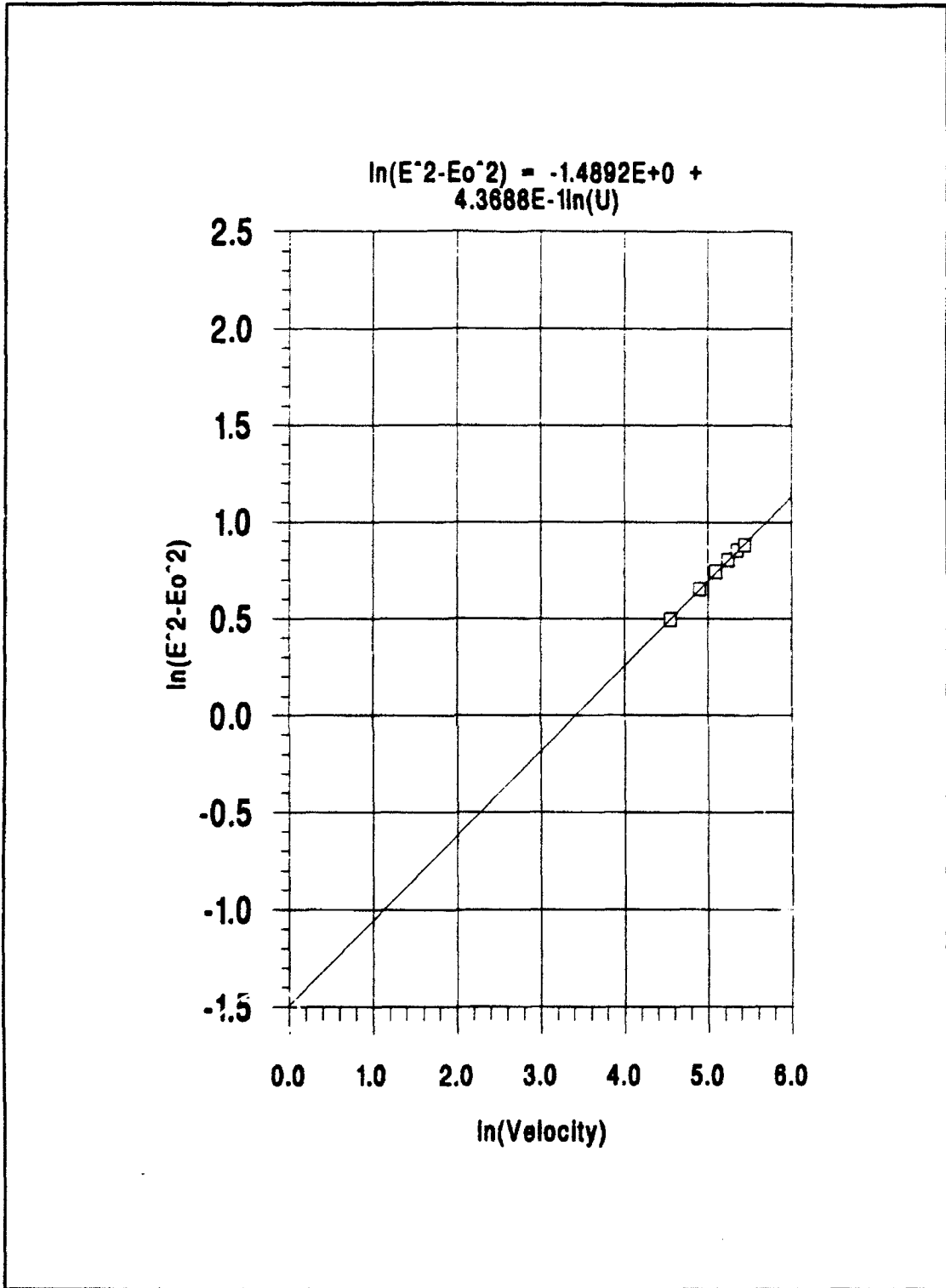


Figure 2.19 Linearized Calibration of Hot Wire



Figure 2.20 Hot Wire Probe

observe the signal. Figure 2.21 is a photograph of the data acquisition equipment.

The output signals were conditioned with the use of a 10000-Hz low-pass filter. Tunnel velocity (\bar{U}) was obtained from the results of the airspeed calibration described in the previous section. Turbulence intensity values were computed using Equation 2.34.

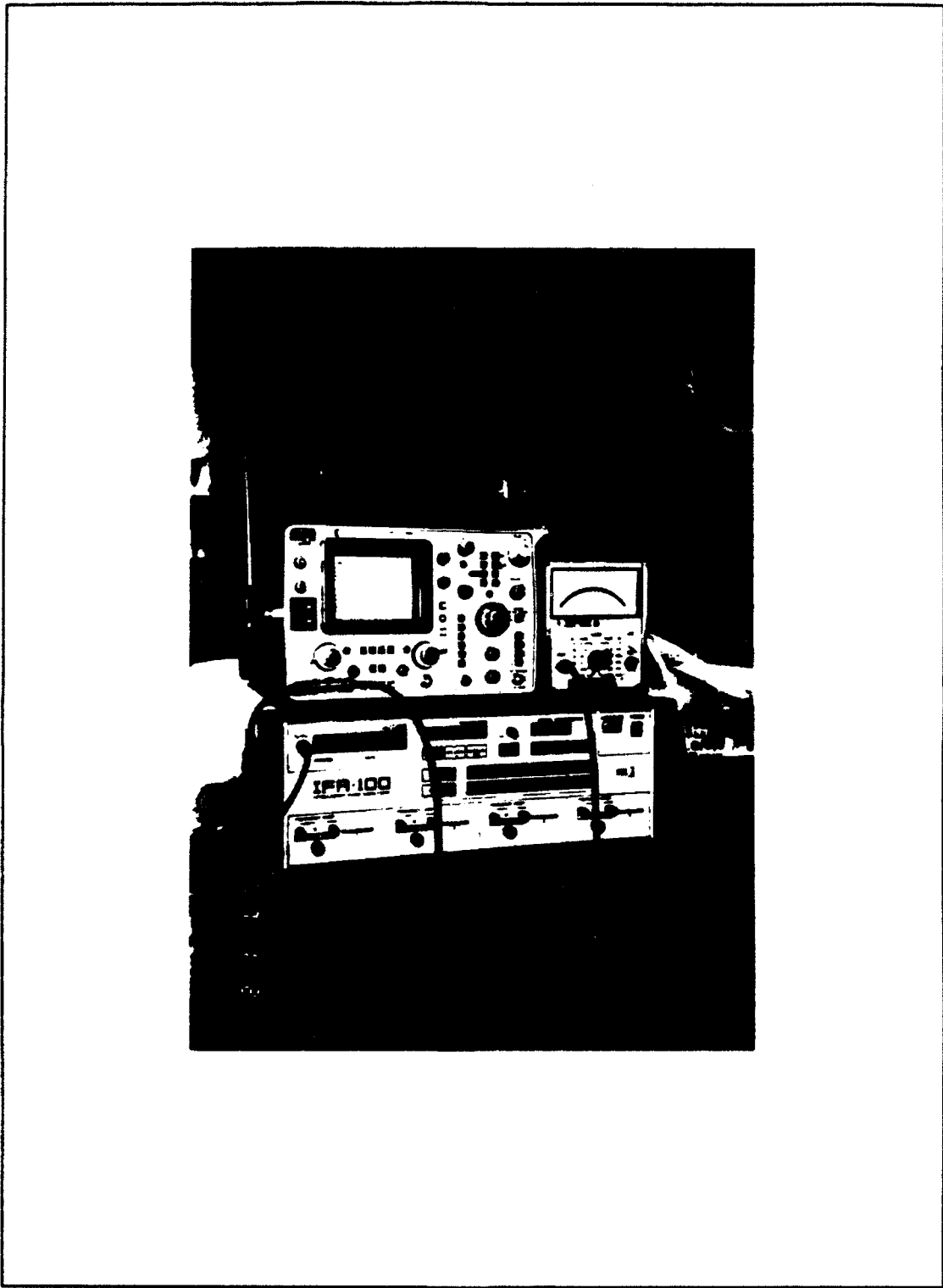


Figure 2.21 Thermal Anemometry Acquisition System

III. RESULTS

A. TUNNEL TEMPERATURE

The description of a flow field would not be complete without characterization of its temperature. During initial operations a noticeable change in temperature within the tunnel was observed.

Heat is added to the airstream at a rate equal to the kinetic energy supplied by the power section via the fan. Without an active cooling system, the total temperature of the airstream will increase until equilibrium is reached. Additional contributions to temperature rise are wall friction, flow separation, turbulence and blockage effects.

The Academic Wind Tunnel is equipped with air exchange doors which permit flushing of the hot tunnel air. The exhaust door is located at the top of the settling chamber and routes the hot tunnel air outside the building. The intake door is located just aft of the test section at the top of the tunnel. The system was designed to operate only when the tunnel was at zero velocity. The air exchange system has seldom been used due to the fact that tunnel operating times have been short in duration. During this calibration only the exhaust door was used to cool the tunnel.

Knowledge of airstream temperature is imperative if

testing involves Reynolds number applications. Reynolds number is defined as

$$R_e = \frac{\rho U x}{\mu} \quad 3.1$$

where x is some characteristic length and μ is the coefficient of viscosity. As the temperature increases, Reynolds number decreases. Using the temperature gauge located in the lower portion of the settling chamber, temperature readings were recorded from tunnel start through a run time of 50.0 minutes at a variety of tunnel dynamic pressures. Figure 3.1 plots the change in temperature during the run time. Each tunnel setting had a period of rapid temperature rise followed by an approximately linear increase of temperature with time. These results were used during the turbulence measurement phase of this calibration and are provided as documentation for future users of the Academic Wind Tunnel.

For the temperature range in which this tunnel operated, the average Reynolds number per characteristic length (R_e/x) was $1.2E6ft^{-1}$. A $10.0^\circ F$ change in tunnel temperature resulted in a change in R_e/x of $3.0E4ft^{-1}$.

B. TOTAL PRESSURE FLUCTUATIONS

While performing the temperature profile just described, excessive fluctuations in total pressure were observed. Below a tunnel dynamic pressure of $30.0 lb_f/ft^2$, the total pressure

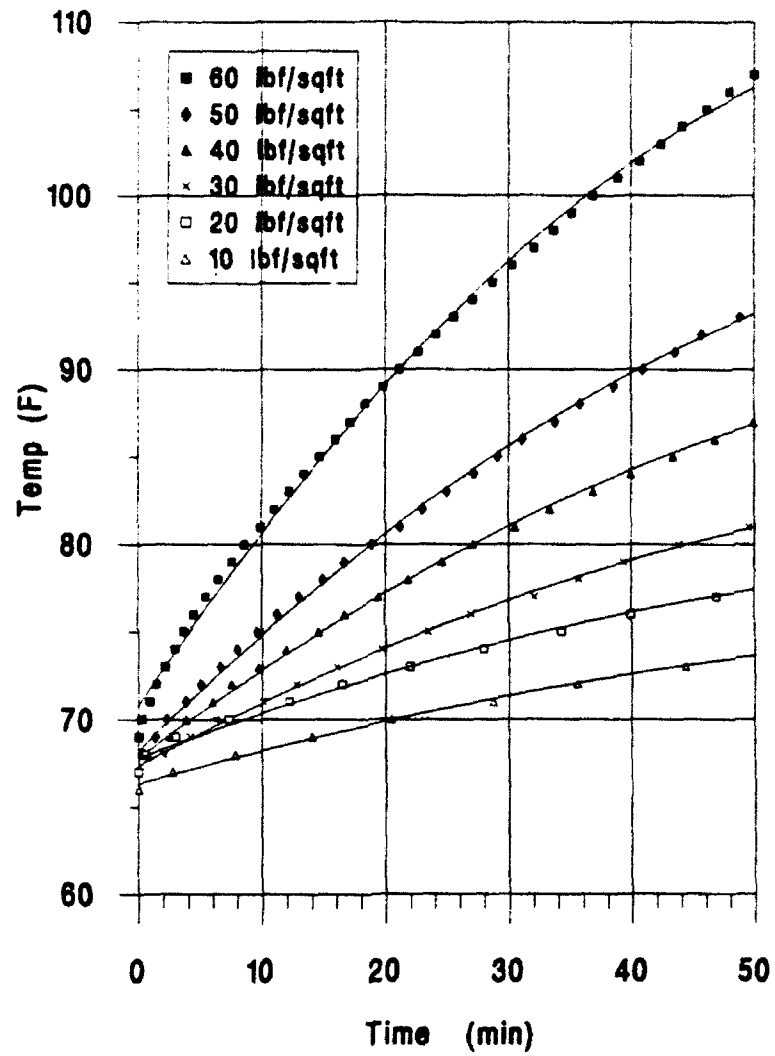


Figure 3.1 Rate of Temperature Change

was constant. Above that setting, fluctuations which increased with dynamic pressure were observed. Two explanations for this condition included pressure losses through leaks in the tunnel and a possible problem of surging caused by flow separation in the diffuser section.

Due to constraints in the design of the diffuser section, the expansion angle was not uniform in the axial direction. This left the boundary layer in this region vulnerable to flow separation. In 1965, splitter plates were positioned in the diffuser section to reduce the diffuser angle. This fixed the periodic separation/reattachment problem that plagued the tunnel in its early years, but whether it completely prevented separation in the diffuser has not been determined.

C. MAXIMUM DYNAMIC PRESSURE

During initial tunnel runs a maximum dynamic pressure of $65.8 \text{ lb}_f/\text{ft}^2$ or 32.17 centimeters of water was obtained. In August 1990 before installation of the damping screen, $71.6 \text{ lb}_f/\text{ft}^2$ or 35.0 centimeters of water was recorded as the maximum dynamic pressure. This $5.8 \text{ lb}_f/\text{ft}^2$ loss in test section dynamic pressure was attributed to the presence of the damping screen. If the Reynolds number used for Equation 1.1 is corrected for the higher velocity flow in the test section, correlation of predicted and actual pressure losses results.

D. LATERAL PRESSURE VARIATION

Due to the width of the mounting bracket, total and static pressure measurements could be recorded no closer than 0.5 of an inch to the tunnel wall. Measurements were recorded from 0.5 through 59.5 inches at one-inch intervals. The 1/16-inch diameter tygon tubing limited measurements to steady state conditions so time was allowed for the conditions to stabilize following probe repositioning.

The Kiel probe was tested to verify its unimpaired accuracy over a range of yaw angles. The probe was rotated forward and backward in the wind tunnel until a change of ± 0.2 of an inch in water height could be observed. This degree of accuracy could be maintained through 51.2° of rotation into the flowstream and 47.1° rotation in the opposite direction.

Figure 3.2 contains the results of the total pressure survey across the test section over a range of tunnel settings. For reclarification, position "0" is the left wall of the tunnel as the probe faced upstream. Figure 3.2 contains three items of interest.

- A general trend of increased total pressure was observed within 10.0 inches of the starboard wall. This difference in energy was audible in the tone of vibration on either side of the contraction cone. It could also be felt by placing a hand through the breather slot on each side of the tunnel and feeling the difference in energy.
- Data acquisition was performed by two people for dynamic pressures up through $50.0 \text{ lb}_f/\text{ft}^2$. One person positioned the probe while the other recorded water height, monitored tunnel temperature and maintained reference dynamic pressure. During the $50.0 \text{ lb}_f/\text{ft}^2$ measurements, it was noted that the fluctuations in total pressure along with

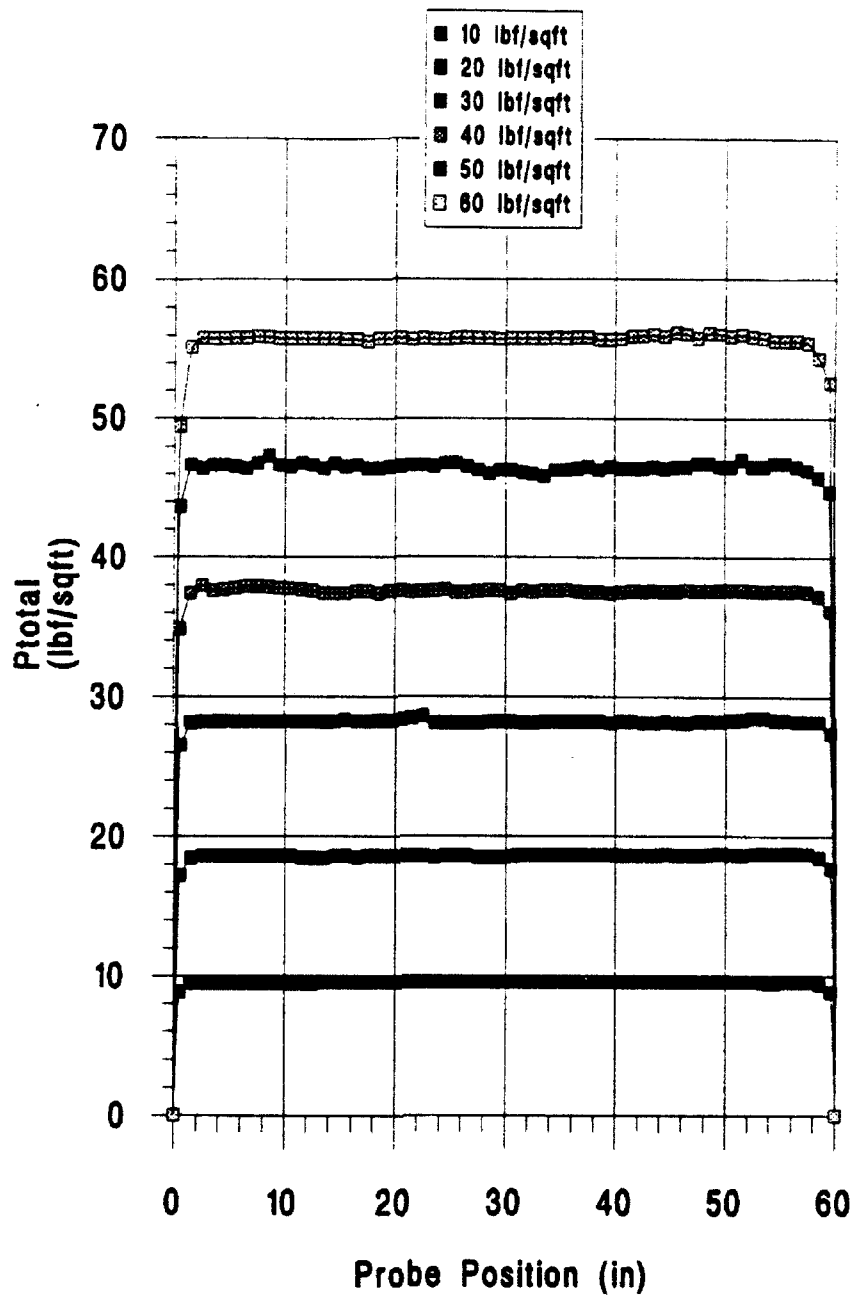


Figure 3.2 Total Pressure Variation

the rapid temperature rise required a third person to monitor the tunnel setting full time. For this reason, the measurement above 50.0 lb_f/ft^2 appears smoother than the one below it.

- The total pressure variation across the tunnel was within 1.0%. This was considered as consistent with the accuracy of the measurement system.

Figure 3.3 graphically represents the total pressure minus the wall static pressure normalized with respect to the tunnel reference dynamic pressure. The activity on the right side of the tunnel is more apparent in this presentation of the data.

The static pressure probe was installed and traversed across the test section during runs of 30.0 lb_f/ft^2 and 50.0 lb_f/ft^2 . As anticipated the static pressure probe showed a significant reaction to the influence of the tunnel wall. In general the trend of the static pressure was to follow the total pressure variation across the test section. Results were within the accuracy of the measurement system. Figure 3.4 presents the static pressure variation normalized with respect to the atmospheric pressure for the runs conducted at the dynamic pressures mentioned.

E. FLOW ANGULARITY

There were two steps involved in the angle of attack calibration of the tunnel balance. The first was to measure the voltage change per degree angle of attack. The second was to adjust the angle limit switches in order to provide the desired range of angle of attack settings. The current

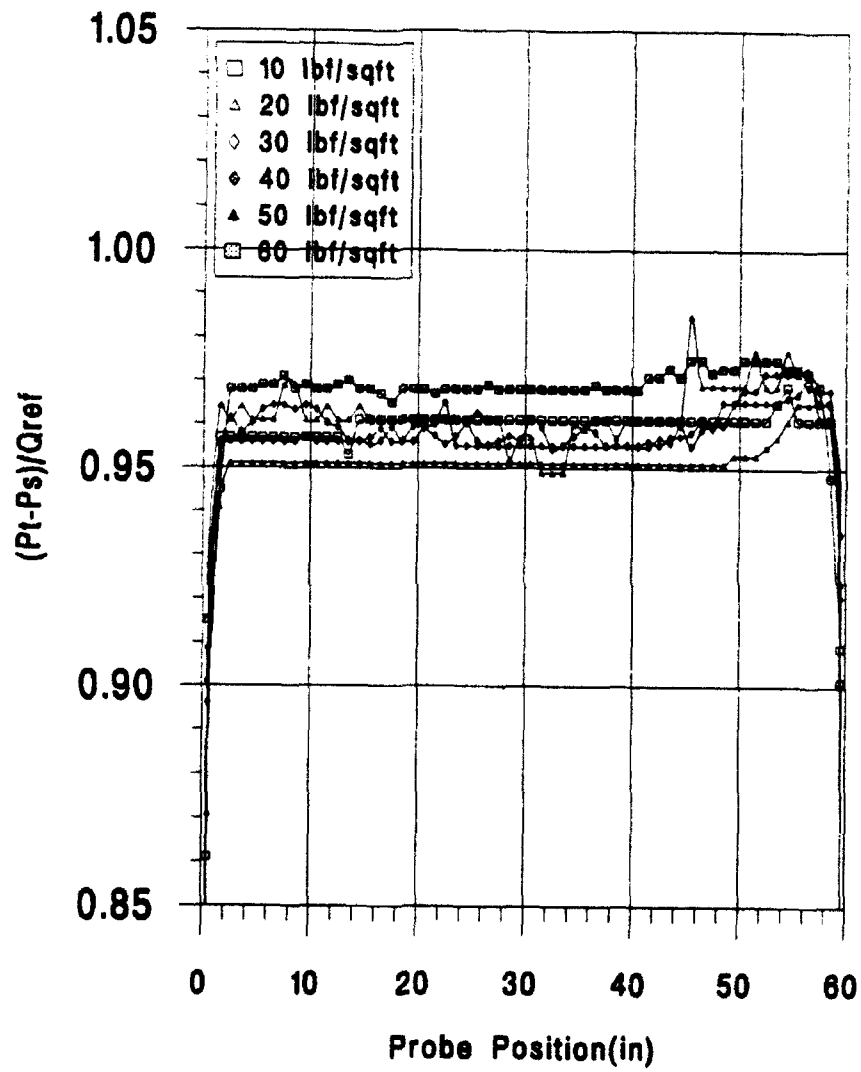


Figure 3.3 Normalized Dynamic Pressure Variation

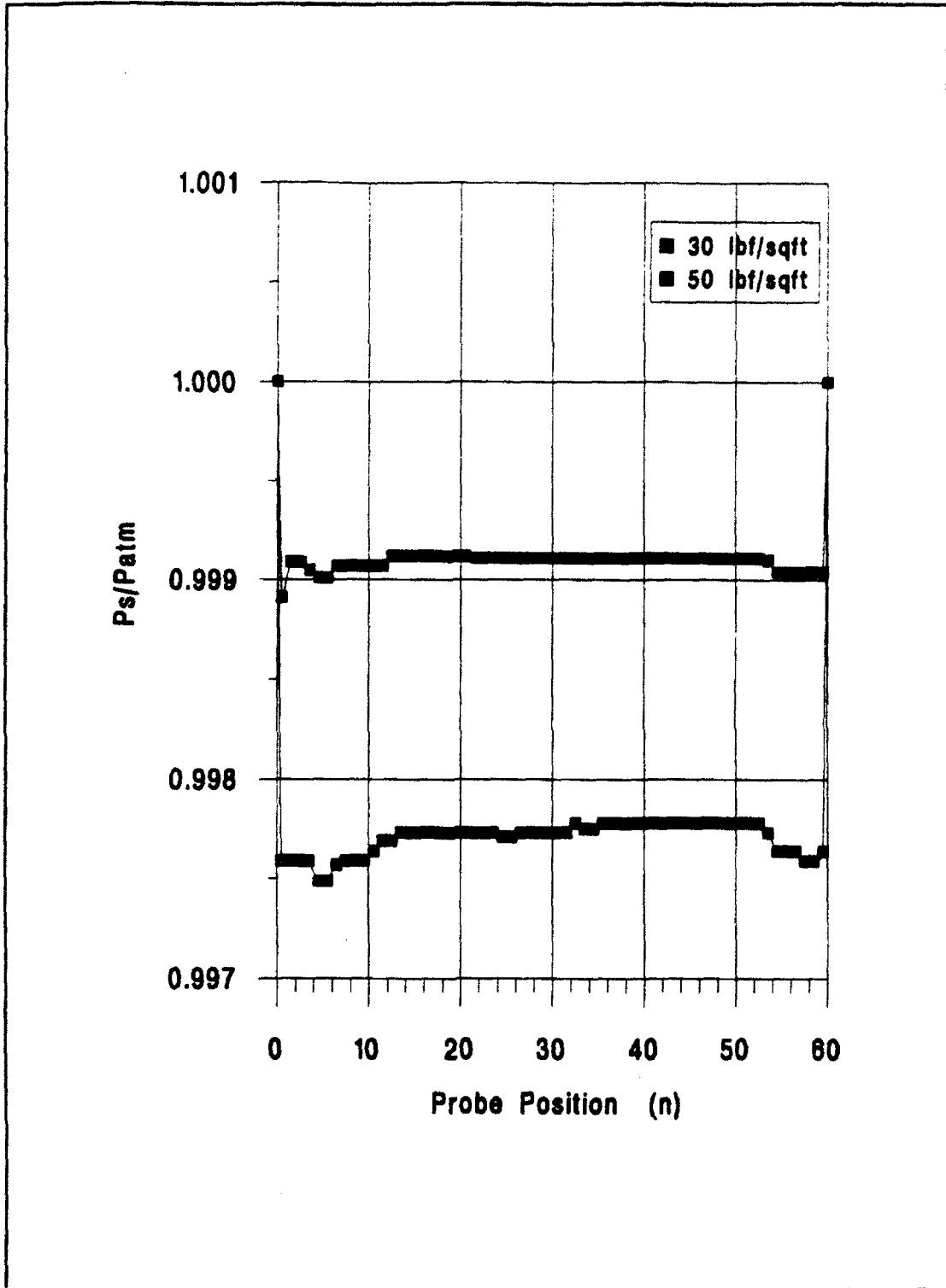


Figure 3.4 Normalized Static Pressure Variation

resistor setup in the automated control system limits the range to $\pm 20.0^\circ$. Figure 3.5 shows 0.48711 volts were required to change the angle of attack setting by one degree. The limit switches were then adjusted to cover a range of settings about the zero geometric angle of attack.

The results of the yawhead calibration at dynamic pressures of $30.0 \text{ lb}_f/\text{ft}^2$ and $50.0 \text{ lb}_f/\text{ft}^2$ are presented in Figures 2.7 through 2.14.

A comparison of theoretical values, calculated using Equation 2.19, to values actually measured during the yawhead calibration was conducted. TABLE 3.1 is a presentation of this comparison.

TABLE 3.1 COMPARISON OF YAWHEAD RESULTS

α (deg)	Theory $\frac{-9/4\sin 2\alpha}{1 - 9/4\sin^2\alpha}$	Actual $\frac{P_{\theta 1} - P_{\theta 3}}{P_{\theta 5} - P_{\infty}}$	Actual $\frac{P_{\theta 2} - P_{\theta 4}}{P_{\theta 5} - P_{\infty}}$
1	-0.0786	-0.114	-0.110
2	-0.1574	-0.171	-0.167
3	-0.2366	-0.228	-0.223
4	-0.3166	-0.286	-0.279
5	-0.3975	-0.343	-0.336

Results from TABLE 3.1 show the difference between theory and actual pressure measurements range from 31.1% at low angles of attack to 15.5% at the higher settings. At

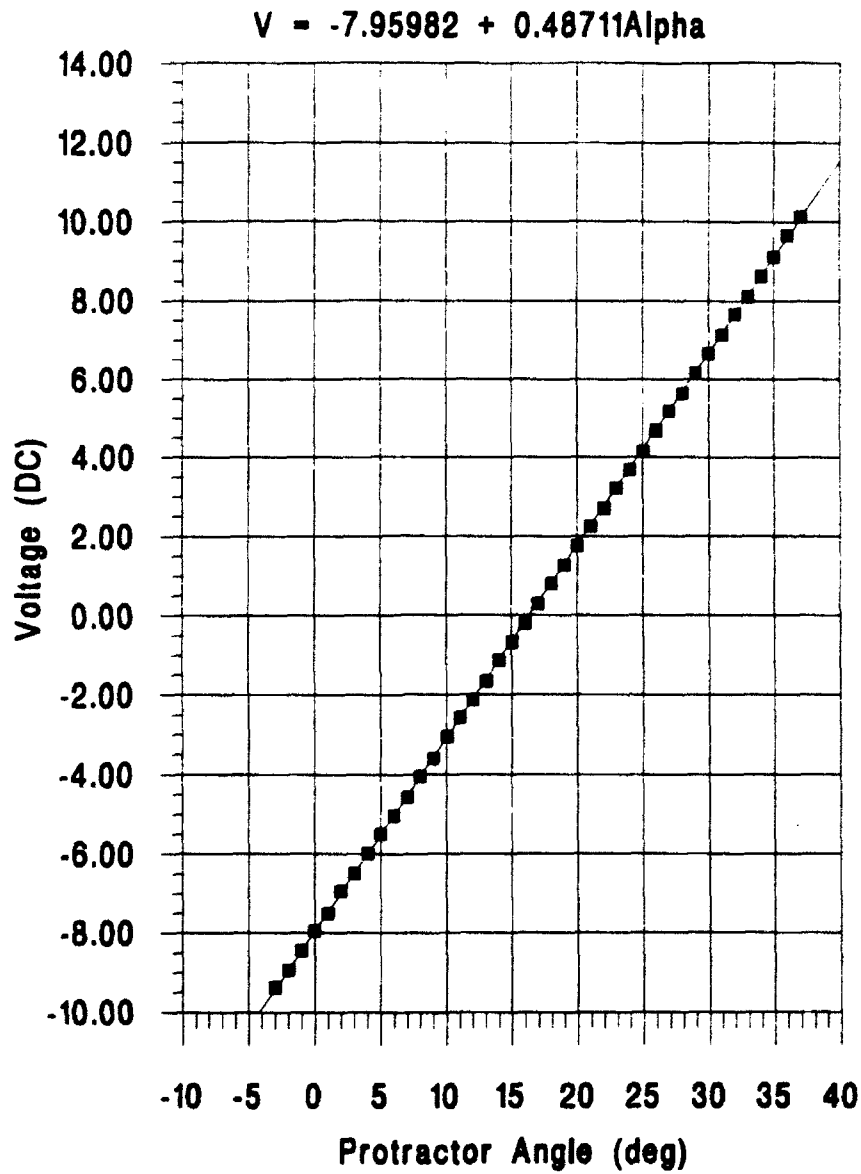


Figure 3.5 Tunnel Balance Angle Calibration

intermediate settings closer correlation exists.

A comparison of the change in pressure relationship with a change in angle of attack revealed values of -0.057 deg^{-1} for the theoretical slope and -0.080 deg^{-1} for the actual slope.

Figures 3.6, 3.7 and 3.8 contain the flow inclination results obtained over a range of dynamic pressures. Three significant features are evident from the results.

- Flow inclination in the horizontal direction is within acceptable limits through the range of dynamic pressures examined.
- The yawhead was traversed 1.25 feet upstream of the calibration position. The results at the lower two speeds confirm flow inclination along the tunnel centerline to be -1.0° . This could not be reproduced at the highest setting. Multiple runs were conducted at all speeds to verify the trend and amount of flow inclination. At the highest speed pressure forces and the significant moment arm created by the yawhead mounting device made it difficult to keep the probe aligned with the flow. This was most pronounced when the probe was near the starboard wall. A torque grip was designed to help stabilize the traversing pole.
- Angular variation of approximately $\pm 1.0^\circ$ exists in the center of the test section at all tunnel settings tested. Due to the airloads and mounting hardware the yawhead vibrated during all readings. This vibration was most pronounced when the yawhead was on the starboard side of the wind tunnel. The erratic readings in this location were repeatable at all speeds.

Two practical methods could be used to reduce the swirl in the test section. Honeycomb placed upstream of the damping screen could reduce the variation in flow angularity. An associated pressure loss across the honeycomb/screen system

$q = 30 \text{ lbf/sqft}$

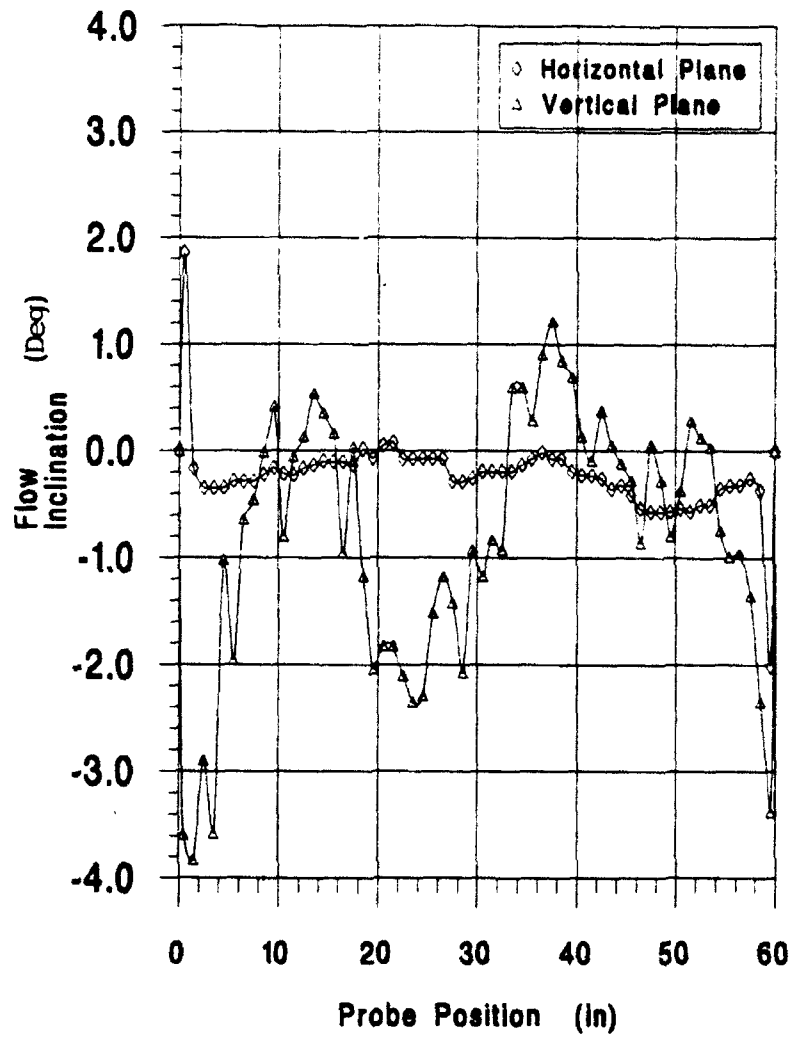


Figure 3.6 Flow Inclination $30 \text{ lb}_f/\text{ft}^2$

$q = 40 \text{ lbf/sqft}$

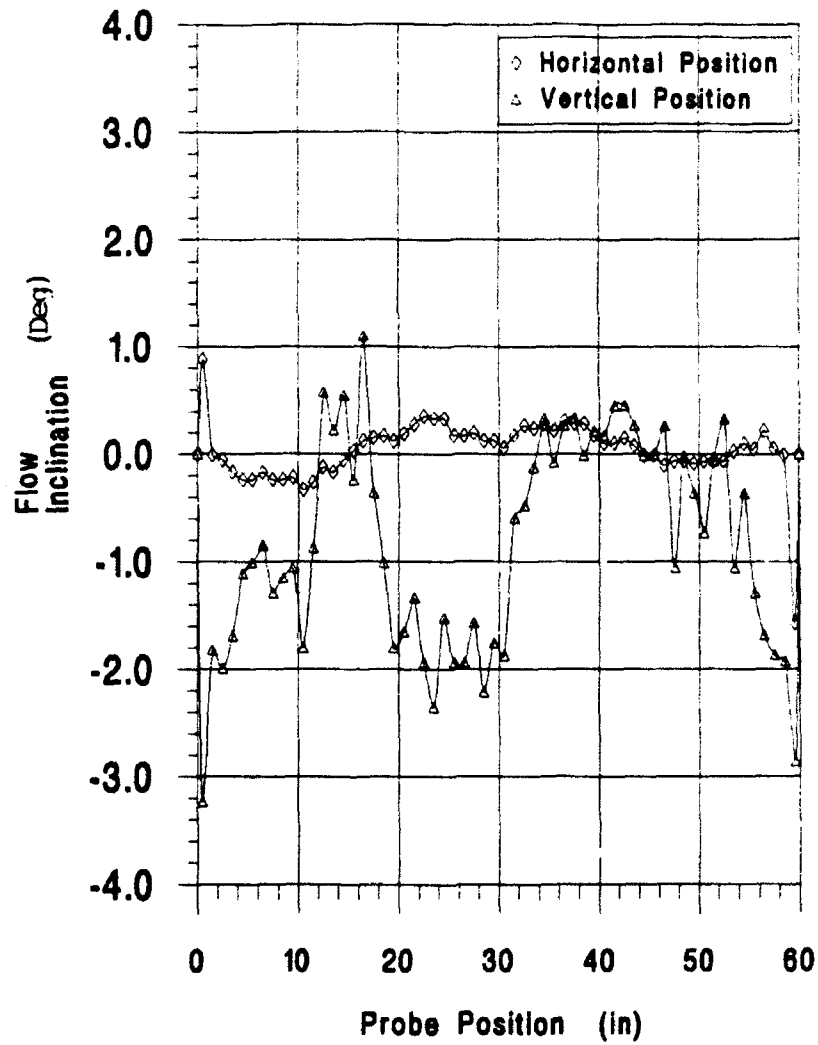


Figure 3.7 Flow Inclination $40 \text{ lb}_f/\text{ft}^2$

$q = 50 \text{ lbf/sqft}$

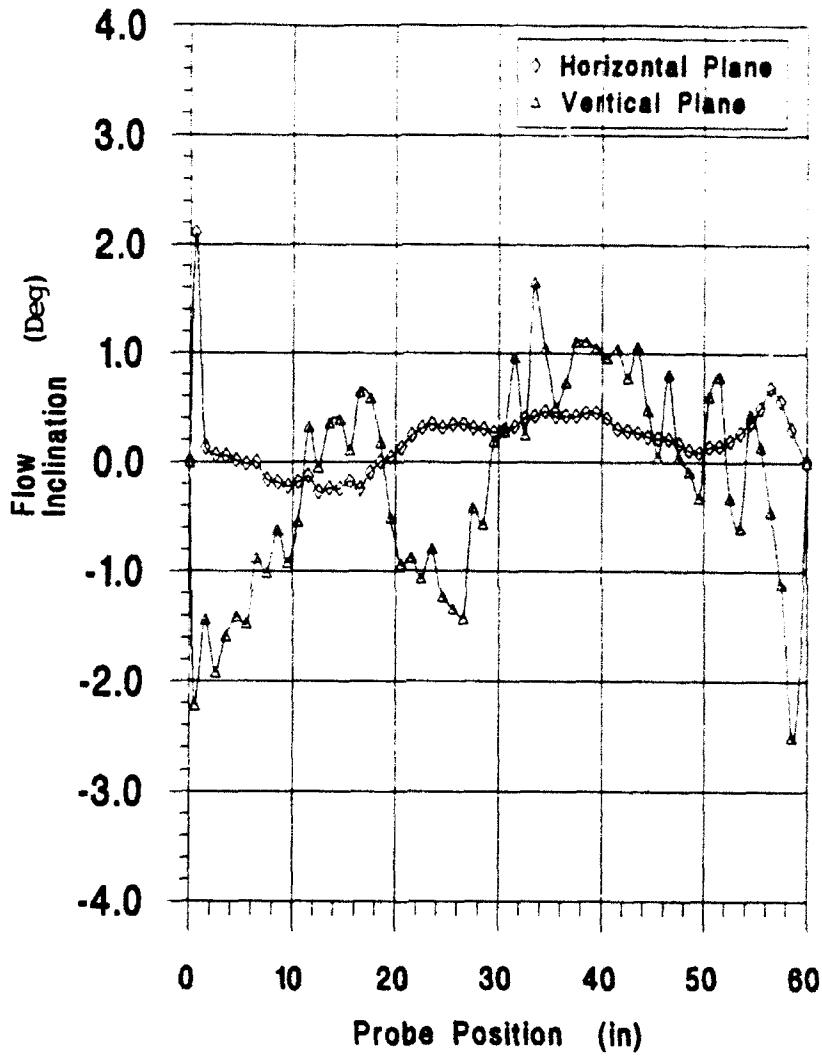


Figure 3.8 Flow Inclination $50 \text{ lb}_f/\text{ft}^2$

would occur. The second method involves adjusting selected trailing edge tabs on the turning vanes upstream of the settling chamber [Ref. 3:p. 64]. This is the most cost-effective procedure to improve flow angularity without increasing pressure losses.

TABLES 3.2 and 3.3 compare the flow inclination before and after the damping screen was installed. Sargent [Ref. 6:p. 22] measured flow angularity at various locations within the test section. His results are used as the "BEFORE" data. Only the lateral position of the "BEFORE" data was documented. The longitudinal location could not be determined, but was assumed to be at the model position.

TABLE 3.2 COMPARISON OF FLOW ANGULARITY AT 30 lb_f/ft²

Probe Location (inches)	Horizontal Plane (degrees)		Vertical Plane (degrees)	
	BEFORE	AFTER	BEFORE	AFTER
3	-0.35	-0.34	-1.19	-1.02
15	-0.57	-0.10	+0.49	+0.16
30	-1.1	-0.19	+0.71	-1.17
45	-1.63	-0.41	+1.41	-0.27
57	-2.5	-0.26	-0.93	-0.95

For orientation, the negative direction refers to flow towards the ceiling in the vertical plane, and towards the zero position in the horizontal plane.

TABLE 3.3 COMPARISON OF FLOW ANGULARITY AT 40 lb_f/ft²

Probe Location (inches)	Horizontal Plane (degrees)		Vertical Plane (degrees)	
	BEFORE	AFTER	BEFORE	AFTER
3	-0.23	-0.17	-1.60	-1.69
15	-0.08	+0.04	-0.30	-0.24
30	-0.53	+0.06	-0.46	-1.80
45	-1.37	-0.01	-0.95	-0.01
57	-0.99	+0.06	-0.80	-1.80

General trends derived from this comparison include the reduction of flow inclination in the horizontal plane, and upward flow along the tunnel centerline following installation of the damping screen.

F. AIRSPEED CALIBRATION

Figure 3.9 contains the results of the airspeed calibration. The vertical axis represents the ratio of the differences in pressure measured with the calibration system to those measured with the reference system, times the compressibility factor. In equation form,

$$\frac{(p_o - p_\infty)_{cal}}{q} = \frac{(p_o - p_\infty)_{cal}}{(p_o - p_\infty)_{ref}} \times \left[1 + \frac{M^2}{4} + \frac{M^4}{40} + \dots \right] \quad 3.2$$

With this current data the tunnel reference system can be used to set the desired velocity conditions at the model position.

Academic Wind Tunnel Calibration 16 October 1992

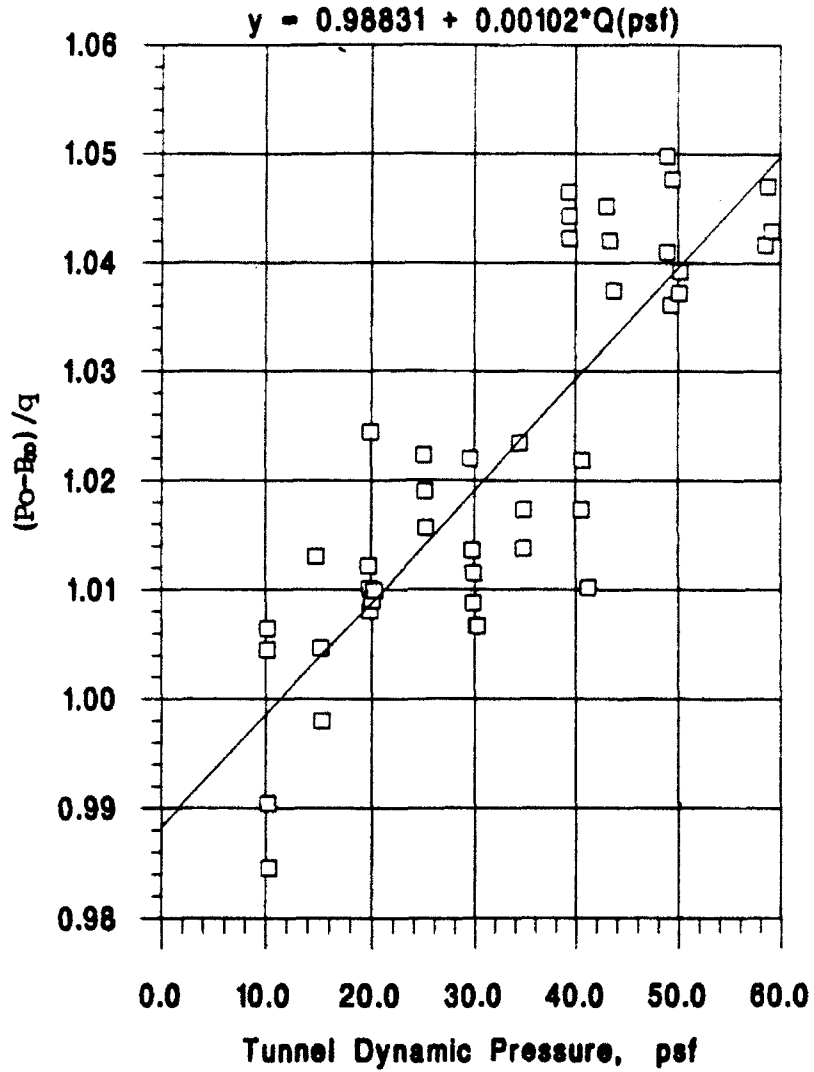


Figure 3.9 Airspeed Calibration

The difference in the diameter of the tygon tubing connecting each system to the micromanometers coupled with the total pressure oscillations already mentioned, made data acquisition difficult. Three readings were taken at a number of selected data points to average the discordant fluctuations.

A potential error in experimental technique was introduced when the calibration pitot-static system was not aligned with the -1.0° flow inclination. The probe was aligned with zero geometric angle of attack. Spacers could have been placed under the rear support to provide proper alignment. Figure 3.10 shows the error introduced by this experimental procedure. In comparison to the accuracy of the measuring system, the error was considered negligible.

G. TURBULENCE INTENSITY

Seven data points were used to calibrate each sensor. To avoid applying temperature compensations to Kings Law, Figure 3.1 was used to select a temperature at which the working fluid would remain constant during calibration. A temperature of 84.0°F or 28.9°C was selected. By varying the tunnel speeds during calibration, the tunnel temperature was maintained at this level. Values for the calibration constants, n and B , were obtained from Figures 2.18 and 2.19 and are listed in TABLE 3.4.

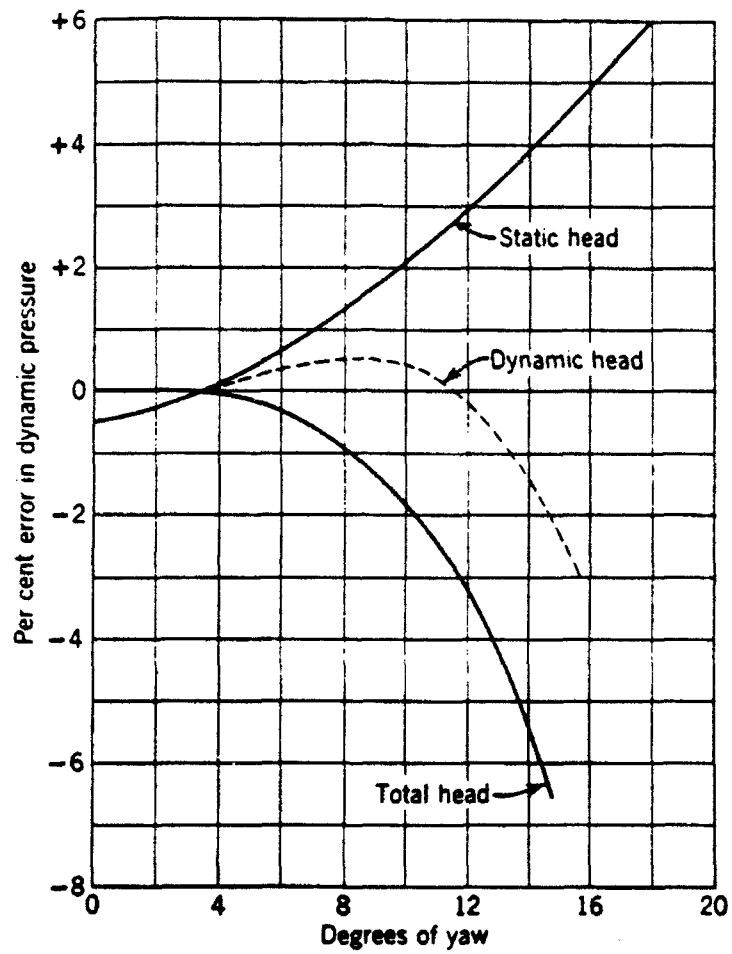


Figure 3.10 Standard Pitot-Static Tube Performance in Yaw

TABLE 3.4 CALIBRATION CONSTANTS

Probe	n	B
Hot Film	0.54	0.43
Hot Wire	0.44	0.23

These calibration constants along with the values for tunnel velocity (\bar{U}), mean voltage (E) and rms voltage ($\sqrt{e'^2}$) were inserted into Equation 2.34 to calculate turbulence intensity. The results along with the result recorded by Nestor [Ref. 1:p. 45] before installation of the damping screen are presented in TABLE 3.5.

TABLE 3.5 TURBULENCE INTENSITY

q (lb _f /ft ²)	Velocity (ft/s)	Turb Int% BEFORE	Turb Int% Hot Film	Turb Int% Hot Wire
10	94.5	-	0.65	0.35
20	133.7	-	1.53	0.40
30	163.7	0.6	1.28	0.43
40	189.0	-	1.19	0.42
50	211.3	-	1.09	0.39
60	231.5	-	1.04	0.34

As discussed in Chapter II, turbulence intensity values include the summation of the axial and vertical velocity perturbations. Table 3.6 reduces the turbulence intensities of TABLE 3.5 by 0.707 on the assumption that the hot-wire anemometer measures both vertical and axial velocity perturbations in a flow field with isotropic turbulence.

TABLE 3.6 LONGITUDINAL TURBULENCE INTENSITY BASED ON ISOTROPIC ASSUMPTION

q (lb _f /ft ²)	Velocity (ft/sec)	Turb Int % BEFORE	Turb Int % Hot Film	Turb Int% Hot Wire
10	94.5	-	0.46	0.25
20	133.7	-	1.08	0.28
30	163.7	0.4	0.91	0.30
40	189.0	-	0.84	0.30
50	211.3	-	0.77	0.28
60	231.5	-	0.74	0.24

Turbulence intensity values are precise to the first decimal place.

Nestor used a hot wire and acquisition system designed by Professor James Miller, a former Naval Postgraduate School professor. Comparison of his result to the results of the hot wire showed a 25.0% to 28.3% reduction in turbulence intensity at a dynamic pressure of 30.0 lb_f/ft².

The difference between the results provided by the hot film and the hot wire was thoroughly investigated. A systematic replacement of various elements of the acquisition system produced similar results. Cables, transducers, even the film probe were replaced. Employees of TSI Incorporated offered helpful advice but maintained the sensors should produce similar results.

Possible explanations for the disparity between the results of the two sensors were reviewed. These included spurious signals of increased eddy shedding due to the larger

diameter of the film probe, and drift in the probe calibration. However, summing all the losses does not account for the significant difference between the values registered by the two sensors.

Bradshaw [Ref. 8:p. 172] describes the errors inherent in the linearization process. These errors have a direct effect on the calibration constants B and n, and thus the values for turbulence intensity. The accuracy of the calibration curve for each sensor was checked. The tunnel was operated at a known speed and values for the dc voltage required to maintain constant sensor temperature were recorded. The velocities corresponding to the recorded voltages were obtained from Figures 2.18 and 2.19. The mean velocity registered by the hot wire exceeded the tunnel speed by 3.9% while the velocity from the hot film differed by 10.7%. This suggested more error was induced by the linearization of the hot film response than that of the hot wire.

IV. CONCLUSIONS/RECOMMENDATIONS

The data obtained was acquired along the vertical centerplane in the test section. It is not implied that a complete mapping of the test section has been performed. Rather, these results document the present condition of the tunnel. Future modifications to the tunnel to further improve the flow quality should reference this material.

A. LATERAL PRESSURE VARIATION

The tunnel is healthy in this regard. Variation of the total and static pressure across the test section is within 1.0% of the mean pressure. Whether or not the damping screen had an effect in this uniform behavior could not be determined since recent documentation in this area could not be found.

B. LONGITUDINAL PRESSURE VARIATION

This phase of the calibration was not performed. The number one priority for future work on the tunnel is to reduce the total head oscillation. A primitive investigation was conducted in this regard. Seams in the high pressure areas within the tunnel were temporarily sealed. Subsequent tunnel operations revealed a decrease in the frequency of small amplitude fluctuations as observed on the reference system micromanometer. A large amplitude low frequency oscillation still remained. The automated pressure reading method and

existing data acquisition system described by Nestor [Ref. 1] should be used to investigate this further. Total and static pressure sensors could be used to obtain time histories of the oscillations for more detailed analysis.

The possibility of separation in the diffuser section should be considered [Ref. 3:p. 121]. Inserting tripping devices through the breather slot would energize the boundary layer forward of the diffuser. An improvement in flow through the diffuser section would be evident by a damping of the total pressure fluctuations.

C. FLOW ANGULARITY

A combination of the current condition of turning vanes and single fan operations without the use of flow straighteners, has produced an angular variation of approximately $\pm 1.0^\circ$ within the test section. Aside from repairing the damaged blades which would increase total pressure, adjustment of the trailing edge tabs on the turning vanes in the settling chamber could remove both the rotation and the -1.0° flow inclination from the test section. With an associated pressure loss, installation of 0.5-inch-thick honeycomb might produce similar results with less speculation.

Consideration must be given to repairing the damaged set of blades. Further modifications may not be necessary if the tunnel is restored to its designed operating condition.

If flow angularity is to be improved by either of the

methods suggested, the system for laterally positioning flow sensors needs to be improved. A more stable system combined with an automated data acquisition system should provide accurate measurements to enable fine adjustment of the turning vanes.

The theory involved in the calibration and operation of the yawhead is consistent with material presented in the introductory aerodynamics course taught within the Aeronautics and Astronautics Department. A laboratory which examines the correlation of theoretical to experimental results would augment the most basic of aerodynamic theories, flow about a sphere.

D. TUNNEL TURBULENCE

The reduction in turbulence intensity was encouraging. The effect of the honeycomb/screen combination would further reduce turbulence in addition to improving flow angularity. Future turbulence measurements should include an examination of the spectral density to identify frequency concentrations in the energy spectrum.

The disparity in results between the hot film and the hot wire remains. One method which was not examined was to place both sensors in the tunnel and simultaneously record data.

E. CLOSING REMARKS

The condition of the tunnel has deteriorated due to neglect. Chipped paint and an occasional piece of cloth tape litter the damping screen. Paint is peeling from the walls of the test section. Technicians who have been employed for years cannot remember the last time the power section was lubricated. Periodic maintenance is required.

Even in its present condition the Academic Wind Tunnel offers a large test section for a wide variety of uses. As student quotas increase, more class laboratories could be conducted in the facility to increase operating time in the Aerolab Wind Tunnel for graduate level research.

Most importantly, there are members of the faculty and staff who are capable and enjoy working with students to improve the flow quality. They liken tunnel calibration to flight testing. Both offer the aerodynamicist an opportunity to incorporate his theoretical background to improve the operational quality of the facility.

LIST OF REFERENCES

1. Nestor, Duanne E., **Calibration of the Naval Postgraduate School 3.5' X 5.0' Academic Wind Tunnel**, Aeronautical Engineer's Thesis, Naval Postgraduate School, Monterey, California, September 1990.
2. Pankhurst, R.C., and Holder, D.W., **Wind Tunnel Technique**, Sir Isaac Pitman & Sons, Ltd, 1952.
3. Pope, Alan, and Harper, John J., **Low-Speed Wind Tunnel Testing**, John Wiley & Sons, Inc., 1966.
4. Naval Postgraduate School, **General Specifications for the 3.5 Ft. x 5.0 Ft. - 200 knot Academic Wind Tunnel**, Enclosure 5, Department of Aeronautics, 1955.
5. Holman, J.P., **Experimental Methods for Engineers**, Fifth Edition, McGraw-Hill, Inc., 1989.
6. Sargent, Christopher L., **The Influence of Helicopter Tail Shape on Drag An Aerodynamic Study Using a Low Speed Wind Tunnel**, Master's Thesis, Naval Postgraduate School, Monterey, California, March 1985.
7. Anderson, John D. Jr., **Fundamentals of Aerodynamics**, Second Edition, McGraw-Hill, Inc., 1991.
8. TSI Incorporated, **IFA 100 System Intelligent Flow Analyzer, Instruction Manual**, Revision C, St. Paul, Minnesota, 1987.
9. Bradshaw, P., **An Introduction to Turbulence and its Measurement**, Pergamon Press, 1971.

INITIAL DISTRIBUTION LIST

1. Defense Technical Information Center 2
Cameron Station
Alexandria, Virginia 22304-6145
2. Library, Code 52 2
Naval Postgraduate School
Monterey, California 93943-5002
3. Professor Daniel J. Collins, Code AA/Co 1
Chairman,
Department Of Aeronautics and Astronautics
Naval Postgraduate School
Monterey, California 93943-5000
4. Professor Louis V. Schmidt, Code AA/Sc 2
Naval Postgraduate School
Monterey, California 93943-5000
5. Professor Richard M. Howard, Code AA/Ho 2
Naval Postgraduate School
Monterey, California 93943-5000
6. Professor Conrad F. Newberry, Code AA/Ne 1
Naval Postgraduate School
Monterey, California 93943-5000
7. Alan G. McGuire, Code AA/Am 2
Naval Postgraduate School
Monterey, California 93943-5000
8. Lt. Robert L. Baldocchi 2
12 Retiro Way
San Francisco, California 94123